

1 Transmembrane helices are an overlooked and
2 evolutionarily conserved source of major
3 histocompatibility complex class I and II epitopes

4 Richèl J.C. Bilderbeek¹, Maksim V. Baranov¹, Geert van den
5 Bogaart¹, and Frans Bianchi¹

6 ¹GBB, University of Groningen, Groningen, The Netherlands

7 November 19, 2021

8 **Abstract**

9 Cytolytic T cell responses are predicted to be biased towards mem-
10 brane proteins. The peptide-binding grooves of most alleles of histocom-
11 patibility complex class I (MHC-I) are relatively hydrophobic, therefore
12 peptide fragments derived from human transmembrane helices (TMHs)
13 are predicted to be presented more often as would be expected based on
14 their abundance in the proteome. However, the physiological reason of
15 why membrane proteins might be over-presented is unclear. In this study,
16 we show that the predicted over-presentation of TMH-derived peptides is
17 general, as it is predicted for bacteria and viruses and for both MHC-I and
18 MHC-II, and confirmed by re-analysis of epitope databases. Moreover,
19 we show that TMHs are evolutionarily more conserved, because single
20 nucleotide polymorphisms (SNPs) are present relatively less frequently in

21 TMH-coding chromosomal regions compared to regions coding for extra-
22 cellular and cytoplasmic protein regions. Thus, our findings suggest that
23 both cytolytic and helper T cells are more tuned to respond to membrane
24 proteins, because these are evolutionary more conserved. We speculate
25 that TMHs are less prone to mutations that enable pathogens to evade T
26 cell responses.

27 **Keywords:** antigen presentation, membrane proteins, bioinformatics, adap-
28 tive immunity, transmembrane domain, transmembrane helix, epitopes, T lym-
29 phocyte, MHC-I, MHC-II, evolutionary conservation

Abbreviations

Abbreviation	Full
ER	Endoplasmatic reticulum
ERAD	ER-associated degradation
HLA	Human leukocyte antigen
IEDB	Immune Epitope Database
LB	lipid body
MAP	Membrane-associated protein
MHC	Major histocompatibility complex
MVB	Multivesicular body
PLC	Peptide-loading complex
SNP	Single nucleotide polymorphism
TMH	Transmembrane helix
TMP	Transmembrane protein

1 Introduction

Our immune system fights diseases and infections from pathogens, such as fungi, bacteria or viruses. An important part of the acquired immune response, that develops specialized and more specific recognition of pathogens than the innate immune response, are T cells which recognize peptides, called epitopes, derived from antigenic proteins presented on Major Histocompatibility Complexes (MHC) class I and II on the cell surface.

The MHC proteins are heterodimeric complexes encoded by the HLA (Human Leukocyte Antigens) genes. In humans, the peptide binding groove of MHC-I is made by only the alpha subunit. There are three classical alleles of MHC-I, hallmarked by a highly polymorphic alpha chain called HLA-A, HLA-B and HLA-C, that all present epitopes to cytolytic T cells. For MHC-II, both the alpha and the beta chains contribute to the peptide binding groove. There are three classical alleles of MHC-II as well, called HLA-DR, HLA-DQ and HLA-DP, that all present epitopes to helper T cells. Each MHC complex can present a subset of all possible peptides. For example, HLA-A and HLA-B have no overlap in which epitopes they bind [1]. Moreover, the HLA genes of humans are highly polymorphic, with hundreds to thousands of different alleles, and each different allele presents a different subset of peptides [2].

Humans express a limited set of MHC alleles and therefore an individual's immune system detects only a fraction of all possible peptide fragments. However, at the population level, the coverage of pathogenic peptides that are detected is very high, because of the highly polymorphic MHC genes. It is therefore believed that MHC polymorphism improves immunity at the population level, as mutations in a protein that disrupt a particular MHC presentation at the individual level, so-called escape mutations, will not affect MHC presentation for all alleles present in the population [3].

58 Many studies are aimed at identifying the repertoire of epitopes that are
59 presented in any of the different alleles to determine which epitopes will result
60 in an immune response, as this will for instance aid the design of vaccines.
61 These studies have led to the development of prediction algorithms that allow
62 for very reliable *in silico* predictions of the peptide binding affinities [4, 5, 6]. For
63 example, S. Tang et al. [6] found that, of the 432 peptides that were predicted
64 to bind to an MHC allele, 86% were experimentally confirmed to do so.

65 Using these prediction algorithms, we recently showed that peptides derived
66 from transmembrane helices (TMHs) are likely to be more frequently presented
67 by MHC-I than expected based on their abundance [7], which is in line with
68 a previous study by Istrail et al [8], demonstrating that N-terminal signal se-
69 quences are likely to be presented within major histocompatibility complexes,
70 due their hydrophobic nature. Moreover, we showed that some well-known im-
71 munodominant peptides stem from TMHs. This over-presentation is attributed
72 to the fact that the peptide-binding groove of most MHC-I alleles is relatively
73 hydrophobic, and therefore hydrophobic TMH-derived peptides have a higher
74 affinity to bind than their soluble hydrophobic counterparts.

75 TMHs are hydrophobic as they need to span the hydrophobic lipid bilayer
76 of cellular membranes. They consist of an alpha helix of, on average, 23 amino
77 acids in length. TMHs can also be predicted with high accuracy from a pro-
78 tein sequence by bioinformatics approaches [9, 10, 11, 12, 13, 14]. For example,
79 a study by Jones [12] found that, from 184 transmembrane proteins (TMPs)
80 with known topology, 80% of the TMH predictions of these proteins matched
81 the experimental findings. TMHs are common structures in the proteins of hu-
82 mans and microbes. Different TMH prediction tools estimate that 15-39% of all
83 proteins in the human proteome contain at least one TMH [15]. However, the
84 physiological reason why peptides derived from TMHs would be presented more

85 often than peptides stemming from soluble (i.e., extracellular or cytoplasmic)
86 protein regions is unknown. In this study, we hypothesized that the presen-
87 tation of TMH residues is evolutionarily preferred, since TMHs are less prone
88 to undergo escape mutations. One reason to expect such a reduced variability
89 (and hence evolutionary conservation) in TMHs, is that these are restricted in
90 their variability by the functional requirement to span a lipid bilayer. This lim-
91 its many of the amino acids present in TMHs to have hydrophobic side chains
92 [16, 17]. Therefore, we speculated that the TMHs of pathogens might have a
93 lower chance to develop escape mutations, as that will result in a dysfunctional
94 TMH and render the protein inactive.

95 This study had two objectives. First, we aimed to generalize our findings
96 by predicting the antigenic presentation from different kingdoms of life in both
97 MHC-I and -II. From these *in silico* predictions, we conclude that TMH-derived
98 epitopes from a human, viral and bacterial proteome are likely to be presented
99 more often than expected by chance for most alleles of MHC-I and II. We con-
100 firmed the presentation of TMH-derived peptides by re-analysis of peptides from
101 The Immune Epitope Database (IEDB) [18]. Second, we tested our hypothe-
102 sis that TMHs are more evolutionary conserved than soluble protein regions.
103 Our analysis of human single nucleotide polymorphisms (SNPs) showed that
104 random point mutations are indeed less likely to occur within TMHs. These
105 findings strengthen the emerging notion that TMHs are important for the T
106 cell-mediated adaptive immune system, and hence are of overlooked importance
107 in vaccine development.

108 2 Methods

109 2.1 Predicting TMH epitopes

110 To predict how frequently epitopes overlapping with TMHs are presented, a sim-
111 ilar analysis strategy was applied as described in [7] for several alleles of both
112 MHC-I and MHC-II, and for a human, viral and bacterial proteome. To sum-
113 marize, for each proteome, all possible 9-mers (for MHC-I) or 14-mers (MHC-II)
114 were derived. For each of these peptides, we determined if it overlapped with a
115 predicted TMH and if it was predicted to bind to the most frequent alleles of
116 each MHC allele.

117 For MHC-I, 9-mers were used, as this is the length most frequently presented
118 in MHC-I and was used in our earlier study [7]. For MHC-II, 14-mers were used,
119 as this is the most frequently occurring epitope length [19]. A human (UniProt
120 ID UP000005640.9606), viral (SARS-CoV-2, UniProt ID UP000464024) and
121 bacterial (*Mycobacterium tuberculosis*, UniProt ID UP000001584) reference pro-
122 teome was used. TMHMM [9] was used to predict the topology of the proteins
123 within these proteomes. To predict the affinity of an epitope to a certain HLA
124 allele, **EpitopePrediction** [7] for MHC-I and **MHCnuggets** [20] for MHC-II was
125 used. Both MHC-I and MHC-II alleles were selected to have a high prevalence
126 in the population, where the alleles of MHC-I are the alleles representing the
127 13 supertypes with over 99.6% coverage of the population’s MHC-I repertoire
128 as defined by [1] [21], and the 21 MHC-II alleles, have a phenotypic frequency
129 of 14% or more in the human population [22].

130 We define a protein to be a binder if, for a certain MHC allele, any of its
131 9-mer or 14-mer peptides have an IC50 value in the lowest 2% of all peptides
132 within a *proteome* (see supplementary Tables S1 and S2 for values), this differs
133 from our previous study where we defined a binder as having an IC50 in the
134 lowest 2% of the peptides within a *protein*. This revised definition precludes

135 bias of proteins that give rise to no or only very few MHC epitopes. To verify
136 that the slight change in method yields similar results, a side by side comparison
137 is shown in the supplementary materials, Figures S1A and S1B.

138 **2.2 TMH epitopes obtained from experimental data**

139 To obtain experimental confirmation that peptides stemming from TMHs are
140 presented by MHC-I and MHC-II, we mined the IEDB [18] for confirmed hu-
141 man MHC-ligands. We queried the IEDB for all linear epitopes obtained from
142 MHC ligand assays in healthy humans, carrying the MHC alleles as used in this
143 study. From these epitopes, we kept those that were present exactly once in the
144 human reference proteome with UniProt ID UP000005640.9606. We predicted
145 the topology of the protein each epitope was found in, using TMHMM [9], from
146 which we concluded if the epitope is overlapping with a TMH with at least 1
147 amino acid.

148 The full analysis can be found at [https://github.com/richelbilderbeek/](https://github.com/richelbilderbeek/bbbq_article_issue_157)
149 [bbbq_article_issue_157](https://github.com/richelbilderbeek/bbbq_article_issue_157).

150 **2.2.1 Evolutionary conservation of TMHs**

151 To determine the evolutionary conservation of TMHs, we first collected human
152 single nucleotide polymorphisms (SNPs) resulting in a single amino acid substi-
153 tution to determine if this occurred within a predicted TMH or not.

154 As a data source, multiple NCBI (<https://www.ncbi.nlm.nih.gov/>) databases
155 were used: the *dbSNP* [23] database, which contains 650 million cataloged non-
156 redundant human variations (called RefSNPs, [https://www.ncbi.nlm.nih.](https://www.ncbi.nlm.nih.gov/snp/docs/RefSNP_about/)
157 [gov/snp/docs/RefSNP_about/](https://www.ncbi.nlm.nih.gov/snp/docs/RefSNP_about/)), and the databases *gene* (for gene names [24])
158 and *protein* (for proteins sequences [25]).

159 The first query was a call to the *gene* database for the term 'membrane

160 protein' (in all fields) for the organism *Homo sapiens*. This resulted in 1,077
161 gene IDs (on December 2020). The next query was a call to the *gene* database
162 to obtain the gene names from the gene IDs. Per gene name, the *dbSNP* NCBI
163 database was queried for variations associated with the gene name. As the
164 NCBI API constrains its users to three calls per second (to assure fair use), we
165 had to limit the extent of our analysis.

166 The number of SNPs was limited to the first 250 variations per gene, resulting
167 in $\approx 61k$ variations. Only variations that result in a SNP for a single amino acid
168 substitution were analyzed, resulting in $\approx 38k$ SNPs. The exact amounts can be
169 found in the supplementary materials, Tables S3 and S4.

170 SNPs were picked based on ID number, which is linked to their discovery
171 date. To verify that these ID numbers are unrelated to SNP positions, the
172 relative positions of all analyzed SNPs in a protein were determined. This
173 analysis showed no positional bias of the SNPs, as shown in supplementary
174 figure S2.

175 Per SNP, the *protein* NCBI database was queried for the protein sequence.
176 For each protein sequence, the protein topology was determined using PureseqTM.
177 Using these predicted protein topologies, the SNPs were scored to be located
178 within or outside TMHs.

179 3 Results

180 3.1 TMH-derived peptides are predicted to be over-presented 181 in MHC-I

182 Figure 1A shows the predicted presentation of TMH-derived peptides in MHC-
183 I, for a human, viral and bacterial proteome. Per MHC-I allele, it shows the
184 percentage of binders that overlap with a TMH with at least one residue. The

horizontal line shows the expected percentage of TMH-derived epitopes that would be presented, if TMH-derived epitopes would be presented just as likely as epitopes derived from soluble regions, when assuming equal incidence of soluble and TMH-derived epitope presentation. For 11 out of 13 MHC-I alleles, TMH-derived epitopes are predicted to be presented more often than the null expectation, for a human and bacterial proteome. For the viral proteome, 12 out of 13 MHC-I alleles present TMH-derived epitopes more often than expected by chance. The extent of the over-presentation between the different alleles is similar for the probed proteomes, which strengthens our previous conclusion [7] that the hydrophobicity of the MHC-binding groove is the main factor responsible for the predicted over-presentation of TMH-derived peptides.

3.2 TMH-derived peptides are predicted to be over-presented in MHC-II

We next wondered if the over-representation of TMH-derived peptides would also be confirmed for MHC-II. Figure 1A shows the percentages of MHC-II epitopes predicted to be overlapping with TMHs for our human, viral and bacterial proteomes. We found that TMH-derived peptides are over-presented in all of the 21 MHC-II alleles, for a human, bacterial and viral proteome, except for HLA-DRB3*0101 in *M. tuberculosis*. See supplementary Table S5 for the exact TMH and epitope counts.

3.3 The over-presentation of TMH-derived peptides is caused by the hydrophobicity of the MHC peptide binding groove

For MHC-I, we previously showed that the over-presentation of TMH-derived peptides is caused by the hydrophobicity of the peptide binding grooves [7]. Fig-

ures 1B and 1C show the extent of over-presentation of TMH-derived epitopes as a function of the hydrophobicity preference score for the different human MHC alleles. An assumed linear correlation explains 88% of the variability in MHC-I. For MHC-II, 62% of the variability is explained by hydrophobicity. This indicates that TMH-derived peptides are over-presented, because the peptide binding grooves of most MHC-I and -II alleles are relatively hydrophobic.

3.4 Experimental validation of presentation of TMH-derived peptides

The Immune Epitope Database (IEDB) from the National Institutes of Health contains millions of linear epitope sequences obtained by MHC ligand assays. For the MHC alleles used in this study, we obtained 54,303 and 2,484 linear epitope sequences for the MHC-I and MHC-II alleles from human origin respectively. There are relatively few epitopes for MHC-II, as MHC-II has many more different alleles than MHC-I, whereas we selected only the human epitopes found for the 21 MHC-II alleles used in this study.

Figure (2A and S3) shows there are similar levels of over-presentation of TMH-derived epitopes between (1) the percentage of TMH-derived epitopes that is reported in the IEDB database versus (2) the percentage of TMH-derived epitopes that is predicted to be presented in MHC-I alleles. For MHC-II alleles, there were too few epitopes per MHC allele to result in an informative figure.

In figure 2B we grouped all the epitopes presented by MHC-I and MHC-II alleles by the percentage of TMH-derived epitopes, which are 22% and 10%, respectively.

These findings robustly confirm that epitopes derived from human TMHs are presented in both MHC-I and MHC-II, and support that they are over-presented. See the supplementary Table S6 for the exact values.

236 We also mined the IEDB database for epitopes for any type of T-cell response
237 from the specified alleles, from the total reports 36% and 7% concerned TMH-
238 derived epitopes in MHC class I and II, respectively (see Figure S4).

239 This data confirms that not only TMH derived epitopes are presented on
240 MHC, but this also elicits T-cell mediated immune responses.

241 **3.5 Human TMHs are evolutionarily conserved**

242 We addressed the question whether there is an evolutionary advantage in pre-
243 senting TMHs. We determined the conservation of TMHs by comparing the
244 occurrences of SNPs located in TMHs or soluble protein regions for the genes
245 coding for membrane proteins. We obtained 911 unique gene names associated
246 with the phrase 'membrane protein', which are genes coding for both membrane-
247 associated proteins (MAPs, which have no TMH) and transmembrane proteins
248 (TMPs, which have at least one TMH). These genes are linked to 4,780 pro-
249 tein isoforms, of which 2,553 are predicted to be TMPs and 2,237 proteins are
250 predicted to be MAPs. We obtained 37,630 unique variations, of which 9,621
251 are SNPs that resulted in a straightforward amino acids substitution, of which
252 6,062 were located in predicted TMPs. See supplementary Tables S3 and S4 for
253 the detailed numbers and distributions of SNPs.

254 Per protein, we calculated two percentages: (1) the percentage of a protein
255 sequence length bearing TMHs, and (2) the percentage of SNPs located within
256 these predicted TMHs. Each percentage pair was plotted in figure 3A. The
257 proportion of SNPs found in TMHs varied from none (i.e., all SNPs were in
258 soluble regions) to all (i.e., all SNPs were in TMHs). To determine if SNPs
259 were randomly distributed over the protein, we performed a linear regression
260 analysis, and added a 95% confidence interval on this regression. This linear fit
261 nearly goes through the origin and has a slope below the line of equality, which

262 shows that less SNPs are found in TMHs than expected by chance.

263 We determined the probability to find the observed amount of SNPs in TMHs
264 by chance, i.e., when assuming SNPs occur just as likely in soluble domains as
265 in TMHs. We used a binomial Poisson distribution, where the number of trials
266 (n) equals the number of SNPs, which is 21,208. The probability of success
267 for the i th TMP (p_i), is the percentage of residues within a TMH per TMP.
268 These percentages are shown as a histogram in figure 3B. The expected number
269 of SNPs expected to be found in TMHs by chance equals $\sum p \approx 4,141$. As
270 we observed 3,803 SNPs in TMHs, we calculated the probability of having that
271 amount or less successes. We used the type I error cut-off value of $\alpha = 2.5\%$. The
272 chance to find, within TMHs, this amount or less SNPs equals $6.8208 \cdot 10^{-11}$. We
273 determined the relevance of this finding, by calculating how much less SNPs are
274 found in TMHs, when compared to soluble regions, which is the ratio between
275 the number of SNPs found in TMHs versus the number of SNPs as expected
276 by chance. In effect, per 1000 SNPs found in soluble protein domains, one finds
277 918 SNPs in TMHs, as depicted (as percentages) in figure 3C.

278 We split this analysis for TMPs containing only a single TMH (so-called
279 single-membrane spanners) and TMPs containing multiple TMHs (multi-membrane
280 spanners). We hypothesized that single-membrane spanners are less conserved
281 than multi-membrane spanners, because multi-membrane spanners might have
282 protein-protein interactions between their TMHs, for example to accommodate
283 active sites, and thus might have additional structural constraints. From the
284 split data, we did the same analysis as for the total TMPs. Figure 4A shows the
285 percentages of TMHs for individual proteins as a function of the percentage of
286 SNPs located in TMHs. For both single- and multi-spanners, a linear regression
287 shows that less SNPs are found in TMHs, than expected by chance.

288 We also determined the probability to find the observed amount of SNPs by

chance in single- and multi-spanners. For single-spanners, we found 452 SNPs in TMH, where ≈ 462 were expected by chance. The chance to observe this or a lower number by chance is 0.319. As this chance was higher than our $\alpha = 0.025$, we consider this no significant effect. For the multi-spanners, we found 3,351 SNPs in TMH, where $\approx 3,678$ were expected by chance. The chance to observe this or a lower number by chance is $8.315841 \cdot 10^{-12}$, which means this number is significantly less as explained by variation. The TMHs of multi-spanners are thus significantly more conserved than soluble protein regions, whereas this is not the case for single-spanners.

Also, for single- and multi-spanners, we determined the relevance of this finding by calculating how much less SNPs are found in TMHs when compared to soluble regions, as depicted in figure 4B. In effect, per 1,000 SNPs found in soluble protein domains, one finds 978 SNPs in TMHs of single-spanners and 911 SNPs in TMHs of multi-spanners.

4 Discussion

Epitope prediction is important to understand the immune system function and for the design of vaccines. In this study, we provide evidence that epitopes derived from TMHs are a major but overlooked source of MHC epitopes. Our bioinformatics predictions indicate that the TMH-derived epitope repertoire is larger than expected by chance for both MHC-I and MHC-II, regardless of the organism. Moreover, reanalysis of MHC-ligands from the IEDB database confirmed the presentation of TMH-derived epitopes. Therefore, it seems likely that TMH-derived epitopes would also result in enhanced T cell responses, although the conservation of TMHs might promote the deletion of T cells responsive to TMH-derived epitopes by central tolerance mechanisms. Finally, our SNP analysis shows that TMHs are evolutionary more conserved than solvent-exposed

315 protein regions.

316 **4.1 Mechanism of MHC presentation of TMH-derived epi-** 317 **topes**

318 Although our data show that TMH-derived epitopes are presented in all clas-
319 sical MHC-I and MHC-II alleles, the molecular mechanisms of how integral
320 membrane proteins are processed for MHC presentation are largely unknown
321 [7]. Most prominently, the fundamental principles of how TMHs are extracted
322 from their hydrophobic lipid environments into the aqueous vacuolar lumen,
323 leading to subsequent proteolytic processing are unresolved.

324 A first possibility is that the extraction of TMPs from the membrane is
325 mediated by the ER-associated degradation (ERAD) machinery. For MHC class
326 I (MHC-I) antigen presentation of soluble proteins, the loading of the epitope
327 primarily occurs at the endoplasmatic reticulum (ER). The chaperones tapasin
328 (TAPBP), ERp57 (PDIA3), and calreticulin (CALR) [26] first assemble and
329 stabilize the heavy and light chains of MHC-I. Later, this complex binds to the
330 transporter associated with antigen processing (TAP) leading to the formation of
331 the so-called peptide-loading complex (PLC). The PLC drives import of peptides
332 into the ER and mediates their subsequent loading into the peptide-binding
333 groove of MHC-I [27]. Membrane proteins first will have to be extracted from
334 the membrane before they become amenable to this MHC-I loading by the
335 PLC. In the ER, this process can be orchestrated by the ERAD machinery,
336 consisting of several chaperones that recognize TMPs, ubiquitinate them, and
337 extract them from the ER membrane into the cytosol (retrotranslocation) for
338 proteasomal degradation [28, 29]. Similar to the peptides generated from soluble
339 proteins, the TMP-derived peptides might then be re-imported by TAP into the
340 ER for MHC-I loading. This ERAD-driven antigen retrotranslocation might be

341 facilitated by lipid bodies (LBs) [30], since LBs can serve as cytosolic sites for
342 ubiquitination of ER-derived cargo [31].

343 A second possibility is that TMPs are proteolytically processed by intramem-
344 brane proteases that cleave TMHs while they are still membrane embedded.
345 Supporting this hypothesis is the well-established notion that peptides gener-
346 ated by signal peptide peptidases (SPPs), an important class of intramembrane
347 proteases that cleave TMH-like signal sequences, are presented on a specialized
348 class of MHC-I called HLA-E [32]. The loading of peptides generated by SPP
349 onto MHC-I does not depend on the proteasome and TAP, possibly because
350 the peptides are directly released into the lumen of the ER [32]. However, this
351 mechanism cannot explain how most membrane proteins can be processed for
352 antigen presentation, because SPPs only cleave TMH-like signal sequences at
353 their C-termini, and N-terminal domains will hence not be removed. Neverthe-
354 less, the presentation of peptides with a high hydrophobicity index was shown
355 to be independent of TAP as well [33], suggesting that the TMH peptides might
356 perhaps be released directly in the ER lumen by other intramembrane proteases.

357 A third possibility is that peptide processing and MHC-loading occur in
358 multivesicular bodies (MVBs) [32]. TMPs can be routed from the plasma mem-
359 brane and other organelles by vesicular trafficking to endosomes. Eventually,
360 these TMPs can be sorted by the endosomal sorting complexes required for
361 transport (ESCRT) pathway into luminal invaginations that pinch off from the
362 limiting membrane and form intraluminal vesicles. This thus results in MVBs
363 where the membrane proteins destined for degradation are located in intralumi-
364 nal vesicles. Upon the fusion of MVBs with lysosomes, the entire intraluminal
365 vesicles including the TMPs are degraded [34]. Via this mechanism, TMPs
366 might well be processed for antigen presentation, particularly since the loading
367 of MHC-II molecules is well understood to occur in MVBs [35, 36, 37]. However,

such processing of membrane proteins in MVBs for antigen presentation poses a problem, because complexes of HLA-DR with its antigen-loading chaperon HLA-DM were only observed on intraluminal vesicles, but not on the limiting membranes of MVBs [37], indicating that epitope loading of MHC-II also occurs at intraluminal vesicles. This observation hence raises the question how the intraluminal vesicles carrying the TMPs destined for antigen presentation can be selectively degraded, while the intraluminal vesicles carrying the MHC-II remain intact. A second problem is that phagosomes carrying internalized microbes lack intraluminal vesicles, and it is hence unclear how TMPs from these microbes would be routed to MVBs for MHC-II loading [37].

Alternatively to the enzymatic degradation of lipids in MVBs by lipases [38, 39], they might be oxidatively degraded by reactions with radical oxygen species produced by the NADPH oxidase NOX2 [40]. This oxidation can result in a destabilization and disruption of membranes [40] and might thereby lead to the extraction of TMPs. Due to the hydrophobic nature of TMHs, however, the extracted proteins will likely aggregate and it is unclear how these aggregates would be processed further for MHC loading.

4.2 Evolutionary conservation of TMHs

In general, one might expect that evolutionary selection shapes an immune system where surveillance is directed towards protein regions essential for the survival, proliferation and/or virulence or pathogenic microbes, as these will be most conserved. In SARS-CoV-2, for example, there is preliminary evidence that the strongest selection pressure is directed upon residues that change its virulence [41]. These regions, however, may only account for a small part of a pathogen's proteome. Additionally, the structure and function of these essential regions might differ widely between different pathogenic proteins. Because of

394 this scarcity and variance in targets, one can imagine that it will be mostly
395 unfeasible to provide innate immune responses against such rare essential protein
396 regions, as suggested in a study on influenza [42], where it was found that the
397 selection pressure exerted by the immune system was either weak or absent.

398 Evolutionary selection of pathogens by a host's immune system, however, is
399 more likely to occur for protein patterns that are general, over patterns that are
400 rare. While essential catalytic sites in a pathogenic proteome might be relatively
401 rare, TMHs are common and thus might be a more feasible target for evolution
402 to respond to. Indeed, we have found the signature of evolution when both
403 factors, that is, TMHs and catalytic sites are likely to co-occur, which is in TMPs
404 that span the membrane at least twice. In contrast to single-spanners, where
405 we found no significant evolutionary conservation, the TMHs of multi-spanners
406 are more evolutionary conserved than soluble protein regions. Likely, the TMHs
407 in many multi-spanners need to interact with each other for correct protein
408 structure and function and they might hence be more structurally constrained
409 compared to the TMHs of single-spanners. Thus, we speculate that the human
410 immune system is more attentive towards TMHs in multi-spanners, as these are
411 evolutionarily more conserved.

412 There have been more efforts to assess the conservation of TMHs, using
413 different methodologies. One such example is a study by Stevens and Arkin [43],
414 in which aligned protein sequence data was used. Also this study found that
415 TMHs are evolutionarily more conserved, as the mean amino acid substitution
416 rate in TMHs is about ten percent lower, which is a similar value as we found.
417 Another example is a study by Oberai, et al. [44] that estimated the conservation
418 scores for TMHs and soluble regions based on alignments of evolutionary related
419 proteins, and also found that TMHs are more conserved, with a conservation
420 score that was 17% higher in TMHs. Note that the last study also found that

421 mutations in human TMHs are likelier to cause a disease, in line with our
422 conclusion that TMHs are more conserved.

423 Together, from this study, two important conclusions can be drawn. First,
424 the MHC over-presentation of TMHs is likely a general feature and predicted to
425 occur for most alleles of both MHC-I and -II and for humans as well as bacterial
426 and viral pathogens. Second, TMHs are genuinely more evolutionary conserved
427 than soluble protein motifs, at least in the human proteome.

428 5 Acknowledgments

429 We thank the Center for Information Technology of the University of Gronin-
430 gen for its support and for providing access to the Peregrine high performance
431 computing cluster. FB is funded by a Veni grant from the Netherlands Orga-
432 nization for Scientific Research (016.Veni.192.026) and an Off-Road Grant from
433 the Dutch Medical Science Foundation (ZonMW 04510011910005). GvdB is
434 funded by a Young Investigator Grant from the Human Frontier Science Pro-
435 gram (HFSP; RGY0080/2018), and a Vidi grant from the Netherlands Orga-
436 nization for Scientific Research (NWO-ALW VIDI 864.14.001). GvdB has re-
437 ceived funding from the European Research Council (ERC) under the European
438 Union’s Horizon 2020 research and innovation programme (grant agreement No.
439 862137).

440 6 Data Accessibility

441 All code, intermediate and final results are archived at [https://github.com/](https://github.com/richelbilderbeek/bbbq_article)
442 [richelbilderbeek/bbbq_article](https://github.com/richelbilderbeek/bbbq_article).

443 7 Authors' contributions

444 RJCB and FB conceived the idea for this research. MVB helped with the
445 proteome analysis of *M. tuberculosis*. RJCB wrote the code. RJCB, MB, GvdB
446 and FB wrote the article.

447 References

- 448 [1] Ole Lund, Morten Nielsen, Can Kesmir, Anders Gorm Petersen, Claus
449 Lundegaard, Peder Worning, Christina Sylvester-Hvid, Kasper Lamberth,
450 Gustav Røder, Sune Justesen, et al. Definition of supertypes for HLA
451 molecules using clustering of specificity matrices. *Immunogenetics*, 55(12):
452 797–810, 2004.
- 453 [2] Steven GE Marsh, ED Albert, WF Bodmer, RE Bontrop, B Dupont,
454 HA Erlich, M Fernández-Viña, DE Geraghty, R Holdsworth, CK Hurley,
455 et al. Nomenclature for factors of the HLA system, 2010. *Tissue antigens*,
456 75(4):291, 2010.
- 457 [3] Simone Sommer. The importance of immune gene variability (MHC) in evo-
458 lutionary ecology and conservation. *Frontiers in zoology*, 2(1):1–18, 2005.
- 459 [4] Mette Voldby Larsen, Alina Lelic, Robin Parsons, Morten Nielsen, Ilka
460 Hoof, Kasper Lamberth, Mark B Loeb, Søren Buus, Jonathan Bramson,
461 and Ole Lund. Identification of CD8+ T cell epitopes in the West Nile
462 virus polyprotein by reverse-immunology using NetCTL. *PloS one*, 5(9),
463 2010.
- 464 [5] Ingrid MM Schellens, Can Kesmir, Frank Miedema, Debbie van Baarle,
465 and José AM Borghans. An unanticipated lack of consensus cytotoxic T

- lymphocyte epitopes in HIV-1 databases: the contribution of prediction programs. *Aids*, 22(1):33–37, 2008.
- [6] Sheila T Tang, Krista E van Meijgaarden, Nadia Caccamo, Giuliana Gugin, Michèl R Klein, Pascale van Weeren, Fatima Kazi, Anette Stryhn, Alexander Zaigler, Ugur Sahin, et al. Genome-based in silico identification of new Mycobacterium tuberculosis antigens activating polyfunctional CD8+ T cells in human tuberculosis. *The Journal of Immunology*, 186(2):1068–1080, 2011.
- [7] Frans Bianchi, Johannes Textor, and Geert van den Bogaart. Transmembrane helices are an overlooked source of Major Histocompatibility Complex Class I epitopes. *Frontiers in immunology*, 8:1118, 2017.
- [8] Sorin Istrail, Liliana Florea, Bjarni V Halldórsson, Oliver Kohlbacher, Russell S Schwartz, Von Bing Yap, Jonathan W Yewdell, and Stephen L Hoffman. Comparative immunopeptidomics of humans and their pathogens. *Proceedings of the National Academy of Sciences*, 101(36):13268–13272, 2004.
- [9] Anders Krogh, Björn Larsson, Gunnar Von Heijne, and Erik LL Sonnhammer. Predicting transmembrane protein topology with a hidden Markov model: application to complete genomes. *Journal of molecular biology*, 305(3):567–580, 2001.
- [10] Lukas Käll, Anders Krogh, and Erik LL Sonnhammer. A combined transmembrane topology and signal peptide prediction method. *Journal of molecular biology*, 338(5):1027–1036, 2004.
- [11] Masafumi Arai, Hironori Mitsuke, Masami Ikeda, Jun-Xiong Xia, Takashi Kikuchi, Masanobu Satake, and Toshio Shimizu. ConPred II: a consensus

- 491 prediction method for obtaining transmembrane topology models with high
492 reliability. *Nucleic acids research*, 32(suppl_2):W390–W393, 2004.
- 493 [12] David T Jones. Improving the accuracy of transmembrane protein topology
494 prediction using evolutionary information. *Bioinformatics*, 23(5):538–544,
495 2007.
- 496 [13] Martin Klammer, David N Messina, Thomas Schmitt, and Erik LL
497 Sonnhammer. MetaTM-a consensus method for transmembrane protein
498 topology prediction. *BMC bioinformatics*, 10(1):314, 2009.
- 499 [14] Qing Wang, Chongming Ni, Zhen Li, Xiufeng Li, Renmin Han, Feng Zhao,
500 Jinbo Xu, Xin Gao, and Sheng Wang. PureseqTM: efficient and accu-
501 rate prediction of transmembrane topology from amino acid sequence only.
502 *bioRxiv*, page 627307, 2019.
- 503 [15] Mamoun Ahram, Zoi I Litou, Ruihua Fang, and Ghaith Al-Tawallbeh.
504 Estimation of membrane proteins in the human proteome. *In silico biology*,
505 6(5):379–386, 2006.
- 506 [16] Tara Hessa, Nadja M Meindl-Beinker, Andreas Bernsel, Hyun Kim, Yoko
507 Sato, Mirjam Lerch-Bader, IngMarie Nilsson, Stephen H White, and Gun-
508 nar Von Heijne. Molecular code for transmembrane-helix recognition by
509 the sec61 translocon. *Nature*, 450(7172):1026–1030, 2007.
- 510 [17] DT Jones, WR Taylor, and JM Thornton. A model recognition approach
511 to the prediction of all-helical membrane protein structure and topology.
512 *Biochemistry*, 33(10):3038–3049, 1994.
- 513 [18] Randi Vita, Swapnil Mahajan, James A Overton, Sandeep Kumar Dhanda,
514 Sheridan Martini, Jason R Cantrell, Daniel K Wheeler, Alessandro Sette,

- 515 and Bjoern Peters. The immune epitope database (iedb): 2018 update.
516 *Nucleic acids research*, 47(D1):D339–D343, 2019.
- 517 [19] Elin Bergseng, Siri Dørum, Magnus Ø Arntzen, Morten Nielsen, Ståle
518 Nygård, Søren Buus, Gustavo A de Souza, and Ludvig M Sollid. Dif-
519 ferent binding motifs of the celiac disease-associated hla molecules DQ2.5,
520 DQ2.2, and DQ7.5 revealed by relative quantitative proteomics of endoge-
521 nous peptide repertoires. *Immunogenetics*, 67(2):73–84, 2015.
- 522 [20] Xiaoshan M Shao, Rohit Bhattacharya, Justin Huang, IK Ashok Sivaku-
523 mar, Collin Tokheim, Lily Zheng, Dylan Hirsch, Benjamin Kaminow, Ash-
524 ton Omdahl, Maria Bonsack, et al. High-throughput prediction of MHC
525 class I and II neoantigens with MHCnuggets. *Cancer Immunology Research*,
526 8(3):396–408, 2020.
- 527 [21] A. Sette and J. Sidney. Nine major hla class i supertypes account for the
528 vast preponderance of hla-a and -b polymorphism. *Immunogenetics*, 50:
529 201–212, 1999.
- 530 [22] Jason Greenbaum, John Sidney, Jolan Chung, Christian Brander, Bjoern
531 Peters, and Alessandro Sette. Functional classification of class II human
532 leukocyte antigen (HLA) molecules reveals seven different supertypes and a
533 surprising degree of repertoire sharing across supertypes. *Immunogenetics*,
534 63(6):325–335, 2011.
- 535 [23] Stephen T Sherry, M-H Ward, M Kholodov, J Baker, Lon Phan, Eliza-
536 beth M Smigielski, and Karl Sirotkin. dbSNP: the ncbi database of genetic
537 variation. *Nucleic acids research*, 29(1):308–311, 2001.
- 538 [24] Garth R Brown, Vichet Hem, Kenneth S Katz, Michael Ovetsky, Craig
539 Wallin, Olga Ermolaeva, Igor Tolstoy, Tatiana Tatusova, Kim D Pruitt,

540 Donna R Maglott, et al. Gene: a gene-centered information resource at
541 NCBI. *Nucleic acids research*, 43(D1):D36–D42, 2015.

542 [25] Eric W Sayers, Tanya Barrett, Dennis A Benson, Evan Bolton, Stephen H
543 Bryant, Kathi Canese, Vyacheslav Chetvernin, Deanna M Church, Michael
544 DiCuccio, Scott Federhen, et al. Database resources of the national center
545 for biotechnology information. *Nucleic acids research*, 39(suppl_1):D38–
546 D51, 2010.

547 [26] Kenneth L Rock, Eric Reits, and Jacques Neefjes. Present yourself! by mhc
548 class i and mhc class ii molecules. *Trends in immunology*, 37(11):724–737,
549 2016.

550 [27] Andreas Blees, Dovile Janulienė, Tommy Hofmann, Nicole Koller, Carla
551 Schmidt, Simon Trowitzsch, Arne Moeller, and Robert Tampé. Structure
552 of the human mhc-i peptide-loading complex. *Nature*, 551(7681):525–528,
553 2017.

554 [28] G Michael Preston and Jeffrey L Brodsky. The evolving role of ubiquitin
555 modification in endoplasmic reticulum-associated degradation. *Biochemical*
556 *Journal*, 474(4):445–469, 2017.

557 [29] Birgit Meusser, Christian Hirsch, Ernst Jarosch, and Thomas Sommer.
558 Erad: the long road to destruction. *Nature cell biology*, 7(8):766–772, 2005.

559 [30] Laurence Bougnères, Julie Helft, Sangeeta Tiwari, Pablo Vargas, Benny
560 Hung-Junn Chang, Lawrence Chan, Laura Campisi, Gregoire Lauvau,
561 Stephanie Hugues, Pradeep Kumar, et al. A role for lipid bodies in the
562 cross-presentation of phagocytosed antigens by mhc class i in dendritic
563 cells. *Immunity*, 31(2):232–244, 2009.

- [31] Toyoshi Fujimoto and Yuki Ohsaki. The proteasomal and autophagic pathways converge on lipid droplets. *Autophagy*, 2(4):299–301, 2006.
- [32] Cláudia C Oliveira and Thorbald van Hall. Alternative antigen processing for mhc class i: multiple roads lead to rome. *Frontiers in immunology*, 6:298, 2015.
- [33] Georg Lautscham, Sabine Mayrhofer, Graham Taylor, Tracey Haigh, Alison Leese, Alan Rickinson, and Neil Blake. Processing of a multiple membrane spanning epstein-barr virus protein for cd8+ t cell recognition reveals a proteasome-dependent, transporter associated with antigen processing-independent pathway. *The Journal of experimental medicine*, 194(8):1053–1068, 2001.
- [34] Jean Gruenberg. Life in the lumen: the multivesicular endosome. *Traffic*, 21(1):76–93, 2020.
- [35] Monique Kleijmeer, Georg Ramm, Danita Schuurhuis, Janice Griffith, Maria Rescigno, Paola Ricciardi-Castagnoli, Alexander Y Rudensky, Ferry Ossendorp, Cornelis JM Melief, Willem Stoorvogel, et al. Reorganization of multivesicular bodies regulates mhc class ii antigen presentation by dendritic cells. *The Journal of cell biology*, 155(1):53–64, 2001.
- [36] Peter J Peters, Jacques J Neefjes, Viola Oorschot, Hidde L Ploegh, and Hans J Geuze. Segregation of mhc class ii molecules from mhc class i molecules in the golgi complex for transport to lysosomal compartments. *Nature*, 349(6311):669–676, 1991.
- [37] Wilbert Zwart, Alexander Griekspoor, Coenraad Kuijl, Marije Marsman, Jacco van Rhee, Hans Janssen, Jero Calafat, Marieke van Ham, Lennert Janssen, Marcel van Lith, et al. Spatial separation of hla-dm/hla-dr inter-

actions within miic and phagosome-induced immune escape. *Immunity*, 22
(2):221–233, 2005.

[38] Peter Sander, Katja Becker, and Michael Dal Molin. Lipase processing of
complex lipid antigens. *Cell chemical biology*, 23(9):1044–1046, 2016.

[39] Martine Gilleron, Marco Lepore, Emilie Layre, Diane Cala-De Paepe,
Naila Mebarek, James A Shayman, Stéphane Canaan, Lucia Mori, Frédéric
Carrière, Germain Puzo, et al. Lysosomal lipases plrp2 and lpla2 process
mycobacterial multi-acylated lipids and generate t cell stimulatory anti-
gens. *Cell chemical biology*, 23(9):1147–1156, 2016.

[40] Ilse Dingjan, Daniëlle RJ Verboogen, Laurent M Paardekooper, Natalia H
Revelo, Simone P Sittig, Linda J Visser, Gabriele Fischer Von Mollard,
Stefanie SV Henriët, Carl G Figdor, Martin Ter Beest, et al. Lipid perox-
idation causes endosomal antigen release for cross-presentation. *Scientific
reports*, 6(1):1–12, 2016.

[41] Lauro Velazquez-Salinas, Selene Zarate, Samantha Eberl, Douglas P
Gladue, Isabel Novella, and Manuel V Borca. Positive selection of ORF3a
and ORF8 genes drives the evolution of SARS-CoV-2 during the 2020
COVID-19 pandemic. *bioRxiv*, 2020.

[42] Alvin X Han, Sebastian Maurer-Stroh, and Colin A Russell. Individual
immune selection pressure has limited impact on seasonal influenza virus
evolution. *Nature ecology & evolution*, 3(2):302–311, 2019.

[43] Timothy J Stevens and Isaiah T Arkin. Substitution rates in α -helical
transmembrane proteins. *Protein Science*, 10(12):2507–2517, 2001.

[44] Amit Oberai, Nathan H Joh, Frank K Pettit, and James U Bowie. Struc-
tural imperatives impose diverse evolutionary constraints on helical mem-

614 brane proteins. *Proceedings of the National Academy of Sciences*, 106(42):
615 17747–17750, 2009.

616 [45] Morten Nielsen, Claus Lundegaard, Thomas Blicher, Bjoern Peters,
617 Alessandro Sette, Sune Justesen, Søren Buus, and Ole Lund. Quantita-
618 tive predictions of peptide binding to any HLA-DR molecule of known
619 sequence: NetMHCIIpan. *PLoS computational biology*, 4(7), 2008.

620 [46] Edita Karosiene, Michael Rasmussen, Thomas Blicher, Ole Lund, Søren
621 Buus, and Morten Nielsen. NetMHCIIpan-3.0, a common pan-specific
622 MHC class II prediction method including all three human MHC class
623 II isotypes, HLA-DR, HLA-DP and HLA-DQ. *Immunogenetics*, 65(10):
624 711–724, 2013.

625 [47] Richèl J C Bilderbeek. tmhmm, 2019. [https://github.com/](https://github.com/richelbilderbeek/tmhmm)
626 [richelbilderbeek/tmhmm](https://github.com/richelbilderbeek/tmhmm) [Accessed: 2019-03-08].

627 [48] Richèl J C Bilderbeek. pureseqtmr, 2020. [https://github.com/](https://github.com/richelbilderbeek/pureseqtmr)
628 [richelbilderbeek/pureseqtmr](https://github.com/richelbilderbeek/pureseqtmr) [Accessed: 2020-05-19].

629 [49] Richèl J C Bilderbeek. netmhc2pan, 2019. [https://github.com/](https://github.com/richelbilderbeek/netmhc2pan)
630 [richelbilderbeek/netmhc2pan](https://github.com/richelbilderbeek/netmhc2pan) [Accessed: 2019-03-08].

631 [50] Richèl J C Bilderbeek. iedbr, 2021. [https://github.com/](https://github.com/richelbilderbeek/iedbr)
632 [richelbilderbeek/iedbr](https://github.com/richelbilderbeek/iedbr) [Accessed: 2021-11-09].

633 [51] Richèl J C Bilderbeek. sprentrez, 2021. [https://github.com/](https://github.com/richelbilderbeek/sprentrez)
634 [richelbilderbeek/sprentrez](https://github.com/richelbilderbeek/sprentrez) [Accessed: 2021-02-09].

635 [52] Richèl J C Bilderbeek. bbbq, 2020. [https://github.com/](https://github.com/richelbilderbeek/bbbq)
636 [richelbilderbeek/bbbq](https://github.com/richelbilderbeek/bbbq) [Accessed: 2020-09-02].

- 637 [53] Steffen Möller, Michael DR Croning, and Rolf Apweiler. Evaluation of
638 methods for the prediction of membrane spanning regions. *Bioinformatics*,
639 17(7):646–653, 2001.
- 640 [54] Claus Lundegaard, Ole Lund, and Morten Nielsen. Prediction of epitopes
641 using neural network based methods. *Journal of immunological methods*,
642 374(1-2):26–34, 2011.
- 643 [55] Morten Nielsen, Claus Lundegaard, Peder Worning, Sanne Lise Lauemøller,
644 Kasper Lamberth, Søren Buus, Søren Brunak, and Ole Lund. Reliable
645 prediction of T-cell epitopes using neural networks with novel sequence
646 representations. *Protein Science*, 12(5):1007–1017, 2003.
- 647 [56] Edita Karosiene, Claus Lundegaard, Ole Lund, and Morten Nielsen.
648 NetMHCcons: a consensus method for the major histocompatibility com-
649 plex class I predictions. *Immunogenetics*, 64(3):177–186, 2012.
- 650 [57] Morten Nielsen, Claus Lundegaard, Peder Worning, Christina Sylvester
651 Hvid, Kasper Lamberth, Søren Buus, Søren Brunak, and Ole Lund. Im-
652 proved prediction of MHC class I and class II epitopes using a novel Gibbs
653 sampling approach. *Bioinformatics*, 20(9):1388–1397, 2004.
- 654 [58] David J. Winter. rentrez: an R package for the NCBI eUtils API. *The R*
655 *Journal*, 9:520–526, 2017.
- 656 [59] Lucia Musumeci, Jonathan W Arthur, Florence SG Cheung, Ashraful
657 Hoque, Scott Lippman, and Juergen KV Reichardt. Single nucleotide dif-
658 ferences (SNDs) in the dbSNP database may lead to errors in genotyping
659 and haplotyping studies. *Human mutation*, 31(1):67–73, 2010.
- 660 [60] Ryan Hunt, Zuben E Sauna, Suresh V Ambudkar, Michael M Gottesman,

661 and Chava Kimchi-Sarfaty. Silent (synonymous) SNPs: should we care
662 about them? *Single nucleotide polymorphisms*, pages 23–39, 2009.

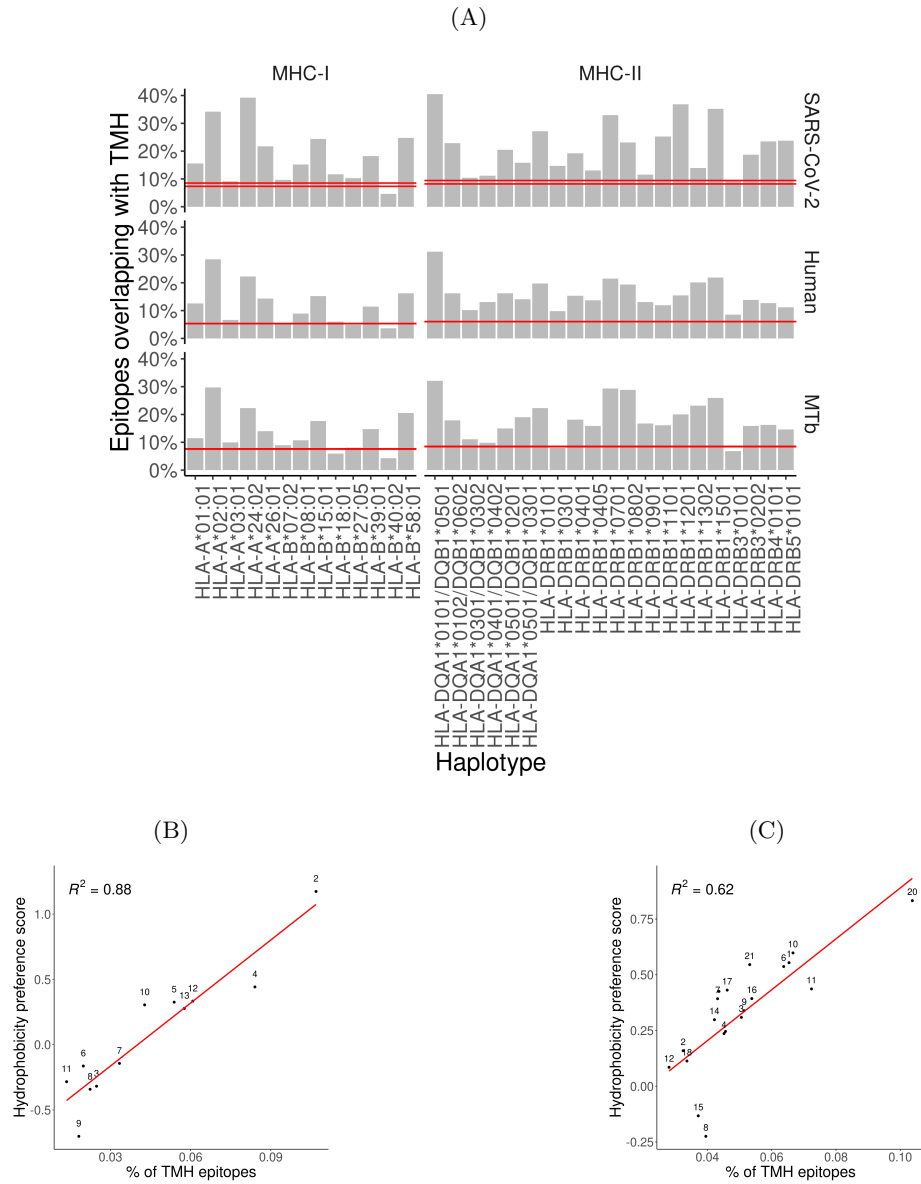


Figure 1: Over-presentation of TMH-derived epitopes on most MHC-I and -II alleles (A) The percentage of epitopes for MHC-I and -II alleles that are predicted to overlap with TMHs for the proteomes of SARS-CoV-2 (top row), human (middle row) and *M. tuberculosis* (MtB; bottom row). The pair of horizontal red lines in each plot indicate the lower and upper bound of the 99% confidence interval. See supplementary Tables S5 and S7 for the exact TMH and epitope counts. **(B-C)** Correlation between the percentages of predicted TMH-derived epitopes and the hydrophobicity score of all predicted epitopes for human MHC-I **(B)** and MHC-II alleles **(C)**. Diagonal red line: linear regression analysis. Labels are shorthand for the HLA alleles, see the supplementary Table S8 for the names.

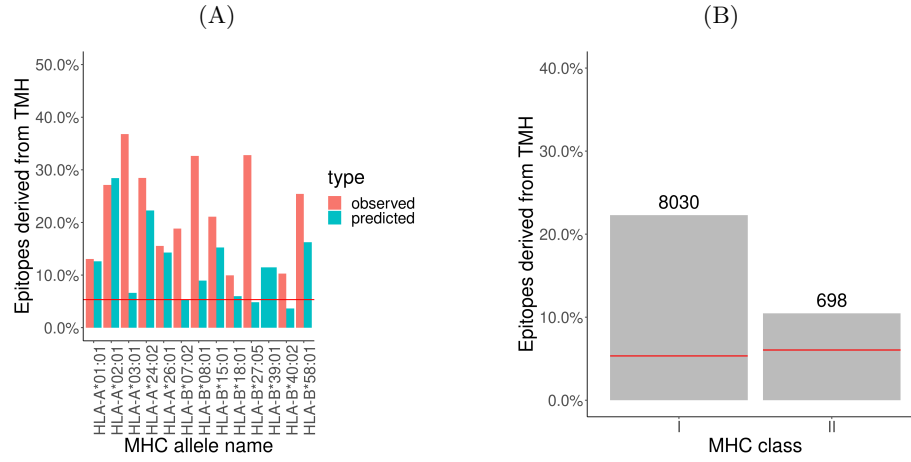


Figure 2: **Analysis of epitope database shows that TMH derived epitopes are over presented.** The percentage of epitopes for MHC-I and -II alleles that overlap with TMHs that are presented. The pair of horizontal red lines in each plot indicate the lower and upper bound of the 99% confidence interval. Note that only one line is visible as this interval is relatively narrow. Alleles are listed in Table S8). **(A)** Observed and predicted percentage of TMH-derived epitopes for MHC-I alleles. **(B)** MHC ligands from IEDB corresponding to TMH-derived epitopes. The numbers above the bars denotes the number of TMH derived epitopes obtained.

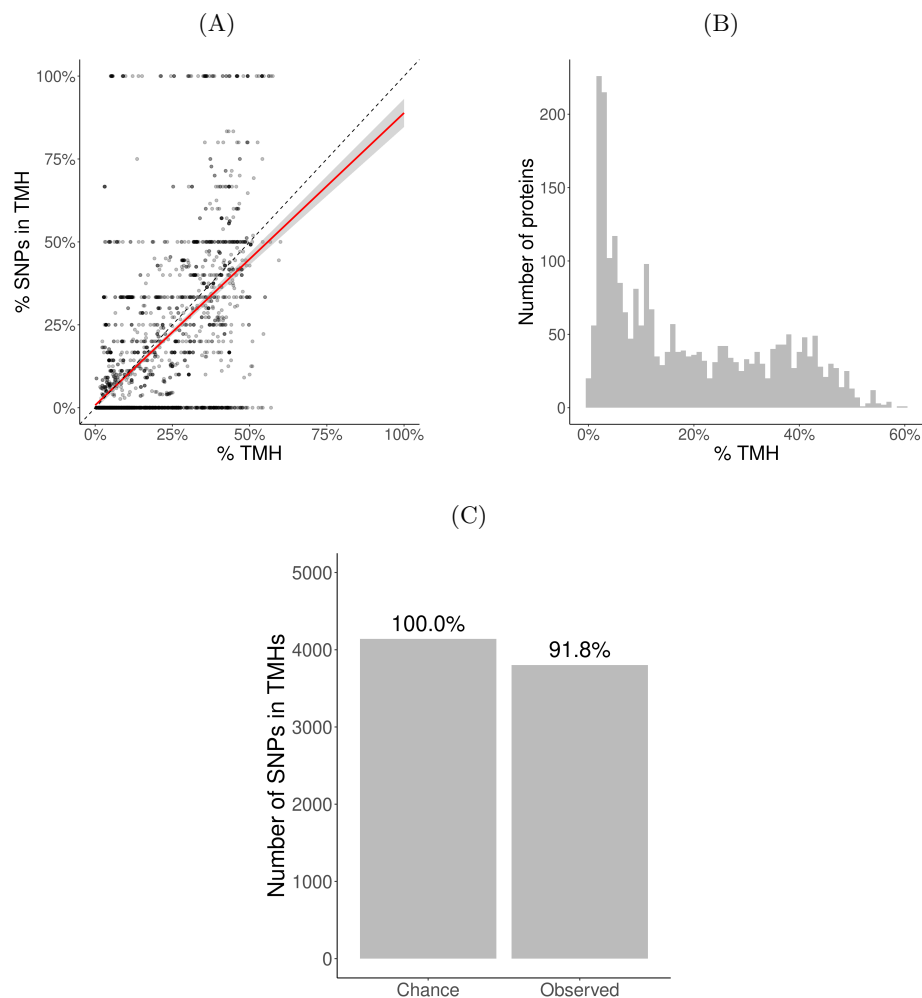


Figure 3: **Evolutionary conservation of human TMHs.** (A) Percentage of SNPs found in TMHs. Each point shows for one protein the predicted percentage of amino acids that are part of a TMH (x -axis) and the observed occurrence of SNPs being located within a TMH (y -axis). The dashed diagonal line shows the line of equality (i.e., equal conservation of TMHs and soluble protein regions). The diagonal red line indicates a linear fit, the gray area its 95% confidence interval. (B) Distribution of the percentages of TMH in the TMPs used in this study. (C) The number of SNPs in TMHs as expected by chance (left bar) and found in the dbSNP database (right bar). Percentages show the relative conservation of SNPs in TMHs found relative to stochastic chance.

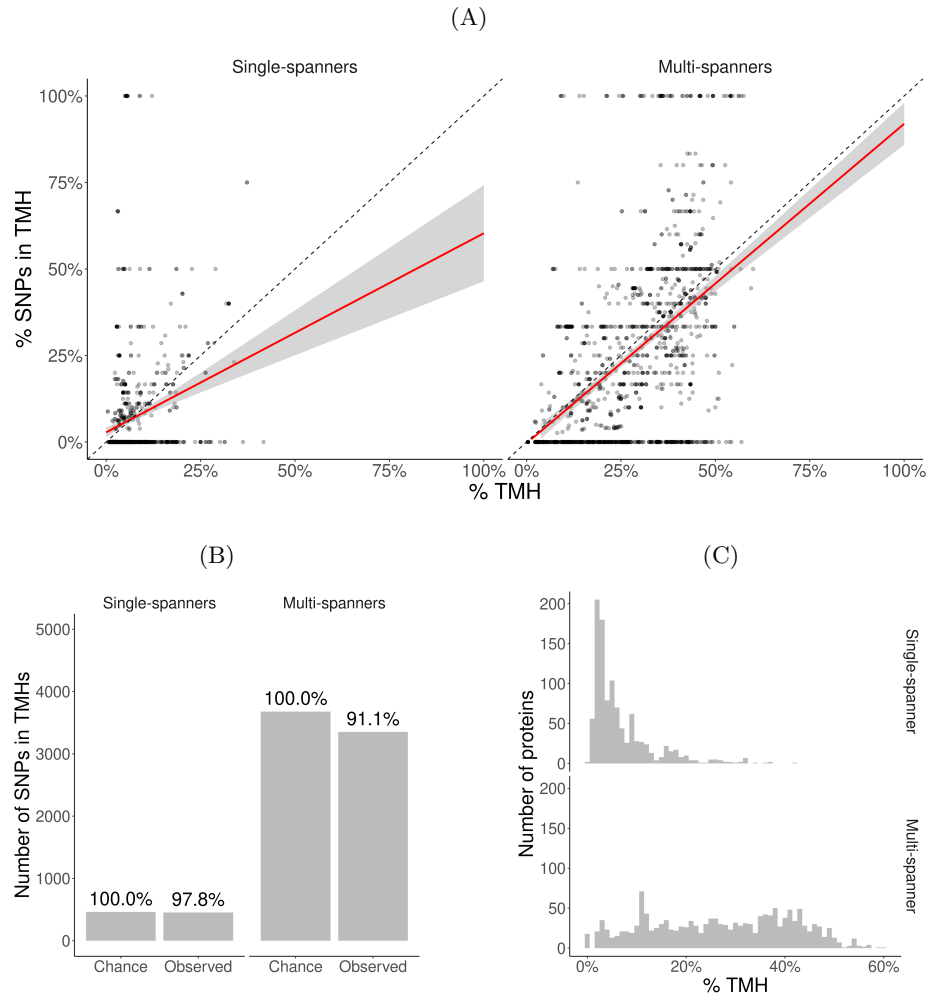


Figure 4: Membrane proteins with multiple TMHs are evolutionary more conserved than proteins with only a single TMH. (A) Percentage of SNPs found in TMPs predicted to have only a single (left) or multiple (right) TMHs. Each point shows for one protein the predicted percentage of amino acids that are part of a TMH (x -axis) and the observed occurrence of SNPs being located within a TMH (y -axis). The dashed diagonal lines show the line of equality (i.e., equal conservation of TMHs and soluble protein regions). The diagonal red lines indicate a linear fit, the gray areas their 95% confidence intervals. (B) The number of SNPs in TMHs as expected by chance and observed in the dbSNP database, for TMPs with one TMH (single-spanners) and multiple TMHs (multi-spanners). Percentages show the relative conservation of SNPs in TMHs found relative to the stochastic chances. (C) Distribution of the proportion of amino acids residing in the plasma membrane.

664 A Supplementary materials

665 A.1 Differences with Bianchi et al., 2017

666 A part of this study does the same analysis as Bianchi et al., 2017. mainly
667 concern the use of different software and a different definition of what an MHC
668 binder is.

669 The earlier study defined a peptide an MHC binder if *within the protein* in
670 which it was found, is was among the peptides with the 2% lowest IC50 val-
671 ues. This can be seen at [https://github.com/richelbilderbeek/bianchi_](https://github.com/richelbilderbeek/bianchi_et_al_2017/blob/master/predict-binders.R)
672 [et_al_2017/blob/master/predict-binders.R](https://github.com/richelbilderbeek/bianchi_et_al_2017/blob/master/predict-binders.R), where the binders are written
673 to file.

674 However, in this study, an MHC binder is defined as a peptide within a
675 *proteome* in which it is found, that is among the peptides with the 2% lowest
676 IC50 values. Subsection A.2 shows the IC50 values for a binder per MHC allele.

677 Our previous study used the TMHMM web server to predict TMHs. The
678 desktop version of TMHMM, however, gives an error message on the 25 seleno-
679 proteins found in the human reference proteome. For the sake of reproducible
680 research, we used the desktop version (as we can call it from scripts) and, due
681 to this, we removed the selenoproteins from this analysis.

682 To verify if the previous and the current method give rise to notable differ-
683 ence, we show a side-by-side comparison in figures S1A and S1B. The figures
684 that MHC molecules that over-present or under-present TMH-derived epitopes,
685 do so in both studies. The extent to which TMH-derived epitopes are presented,
686 however, is more extreme in our current setup.

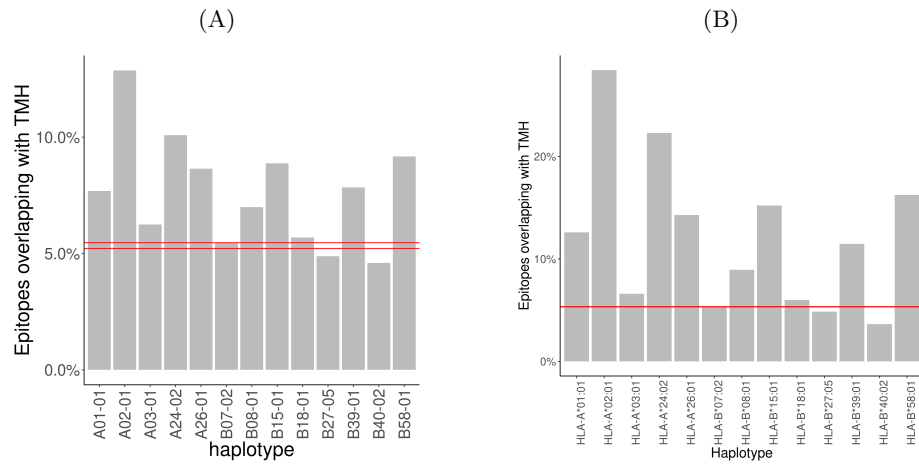


Figure S1: **(A)** Results for [7]. Dashed lines denotes the coincidence interval. **(B)** Results for this study. Dashed line denotes the percentage as expected by chance.

Table S1: IC50 values (in nM) per haplotype below which a peptide is considered a binder. percentage used: 2

haplotype	covid	human	myco
HLA-A*01:01	1470.5912	2545.9537	2812.1714
HLA-A*02:01	118.9596	218.7274	186.7565
HLA-A*03:01	537.0144	804.7455	1544.1073
HLA-A*24:02	984.8147	1590.0623	1971.8258
HLA-A*26:01	1095.2591	1771.6924	1526.1101
HLA-B*07:02	1215.7734	705.6514	435.5361
HLA-B*08:01	886.5661	883.0951	1023.2213
HLA-B*18:01	921.4157	1063.2215	1319.0445
HLA-B*27:05	1186.0963	689.8815	475.6130
HLA-B*39:01	437.3506	484.3843	399.3873
HLA-B*40:02	585.6308	541.2392	600.1688
HLA-B*58:01	435.4693	591.0526	538.9063
HLA-B*15:01	281.9129	440.6541	482.8369

A.2 IC50 values of binders per MHC allele

Per target proteome (i.e. human, SARS-CoV-2, *M tuberculosis*), we collected all 9-mers (for MHC-I) and 14-mers (for MHC-II), after removing the selenoproteins and proteins that are shorter than the epitope length. From these epitopes, per MHC allele, we predicted the IC50 (in nM) using `epitope-prediction` (for MHC-I) and `MHCnuggets` (for MHC-II). Here, we show the IC50 value per MHC allele that is used to determine if a peptide binds to the allele's MHC for MHC-I (see supplementary Table S1) and MHC-II (see supplementary Table S2).

Table S2: IC50 values (in nM) per haplotype below which a peptide is considered a binder. percentage used: 2

haplotype	covid	human	myco
HLA-DRB1*0101	7.3896	9.72	9.9600
HLA-DRB1*0301	121.8420	198.40	164.4900
HLA-DRB1*0401	59.8780	74.92	84.3112
HLA-DRB1*0405	46.2324	51.88	66.7100
HLA-DRB1*0701	17.7464	22.40	28.1700
HLA-DRB1*0802	99.7592	137.16	67.9900
HLA-DRB1*0901	42.3464	53.52	41.5400
HLA-DRB1*1101	35.9988	39.01	48.9200
HLA-DRB1*1201	194.4408	248.72	289.7300
HLA-DRB1*1302	21.1084	40.59	35.4100
HLA-DRB1*1501	32.6196	40.69	46.6700
HLA-DRB3*0101	175.2984	298.94	218.7300
HLA-DRB3*0202	176.8168	291.95	405.8724
HLA-DRB4*0101	47.6384	51.04	62.7800
HLA-DRB5*0101	32.8872	43.52	60.2312
HLA-DQA1*0501/DQB1*0201	193.1108	209.89	174.2124
HLA-DQA1*0501/DQB1*0301	51.2028	43.47	20.3200
HLA-DQA1*0301/DQB1*0302	361.8180	365.96	296.4712
HLA-DQA1*0401/DQB1*0402	214.1932	242.68	199.8912
HLA-DQA1*0101/DQB1*0501	550.4488	674.95	930.9612
HLA-DQA1*0102/DQB1*0602	157.4480	174.82	114.3512

Table S3: Amounts. raw = all variations, including DNA variations. all_proteins = all proteins. map = membrane associated protein. tmp = transmembrane protein. in_tmh = in transmembrane helix of TMP. in_sol = in soluble region of TMP.

what	raw	all_proteins	map	tmp	in_tmh	in_sol
Number of variations	60931	37831	16623	21208	3803	17405
Number of unique variations	60544	37630	16606	21024	3789	17235
Number of unique SNPs	NA	9621	4219	6026	1140	4936
Number of unique gene names	953	911	457	605	325	590
Number of unique protein names	5163	4780	2227	2553	1280	2467
Percentage TMH	NA	10	0	19	26	18

Table S4: Amounts. single_in_tmh = in transmembrane helix of single-spanner. single_in_sol = in soluble region of single-spanner. multi_in_tmh = in transmembrane helix of multi-spanner. multi_in_sol = in soluble region of multi-spanner.

what	single_in_tmh	single_in_sol	multi_in_tmh	multi_in_sol
Number of variations	452	7734	3351	9671
Number of unique variations	451	7733	3338	9502
Number of unique SNPs	160	2393	994	2762
Number of unique gene names	96	282	243	344
Number of unique protein names	304	1032	976	1435
Percentage TMH	11	5	35	26

A.3 Counts

See supplementary Tables S3 and S4 for an overview of all amounts. Note that, for the analyses using the SARS-CoV-2 virus proteome, we labeled this by its disease (covid) to prevent typos. In supplementary Table S3 there are multiple instances where the amounts are expected to add up, yet don't, as one SNP can work on multiple isoforms. For example, there are 9,621 unique SNPs found in all proteins, of which 4,219 around found in MAPs and 6,026 in TMPs. Apparently, 624 SNPs work on a set of isoforms that contains both MAPs and TMPs.

705 A.4 Relative positions

706 See Supplementary Figure S2 for the distribution of the relative position of the
707 SNPs.

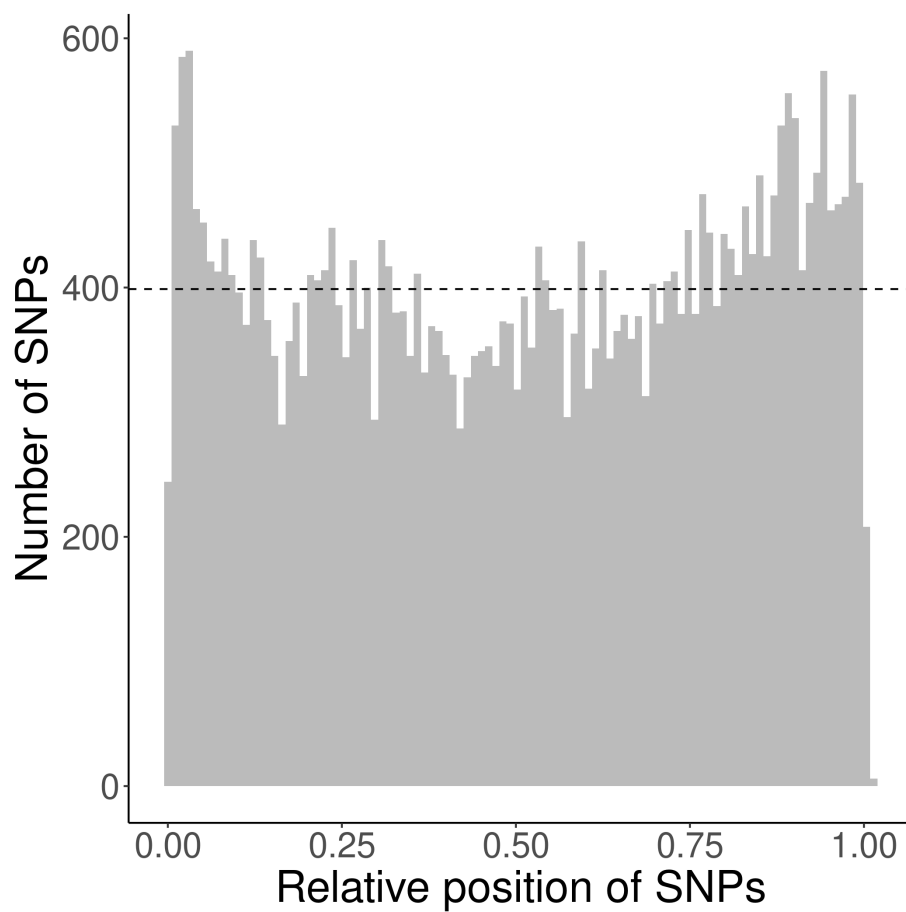


Figure S2: Distribution of the relative position of the SNPs used, where a relative position of zero denotes the first amino acid at the N-terminus, where a relative position of one indicates the last residue at the C-terminus.

Table S5: Percentage of MHC-II 14-mers overlapping with TMH. Values in brackets show the number of binders that have at least one residue overlapping with a TMH (first value) as well as the number of binders (second value). percentage used: 2

haplotype	covid	human	myco
HLA-DQA1*0101/DQB1*0501	40.433 (112/277)	31.214 (69752/223464)	32.158 (8187/25459)
HLA-DQA1*0102/DQB1*0602	22.910 (74/323)	16.167 (35753/221147)	17.950 (4608/25671)
HLA-DQA1*0301/DQB1*0302	10.381 (30/289)	10.179 (22623/222248)	11.144 (2842/25502)
HLA-DQA1*0401/DQB1*0402	11.111 (32/288)	13.135 (29319/223219)	9.890 (2524/25522)
HLA-DQA1*0501/DQB1*0201	20.430 (57/279)	16.240 (36186/222820)	14.999 (3823/25489)
HLA-DQA1*0501/DQB1*0301	15.808 (46/291)	14.106 (31046/220089)	18.969 (4878/25715)
HLA-DRB1*0101	27.119 (80/295)	19.774 (43968/222349)	22.293 (5692/25533)
HLA-DRB1*0301	14.676 (43/293)	9.801 (21831/222752)	7.956 (2025/25451)
HLA-DRB1*0401	19.231 (55/286)	15.325 (34011/221930)	18.113 (4641/25623)
HLA-DRB1*0405	12.996 (36/277)	13.684 (30380/222012)	15.837 (4036/25484)
HLA-DRB1*0701	32.877 (96/292)	21.512 (47856/222465)	29.304 (7471/25495)
HLA-DRB1*0802	23.132 (65/281)	19.339 (42859/221623)	28.805 (7358/25544)
HLA-DRB1*0901	11.565 (34/294)	13.111 (29043/221520)	16.798 (4301/25605)
HLA-DRB1*1101	25.197 (64/254)	11.924 (26582/222928)	16.103 (4101/25467)
HLA-DRB1*1201	36.897 (107/290)	15.482 (34596/223464)	20.018 (5098/25467)
HLA-DRB1*1302	13.962 (37/265)	20.121 (44798/222646)	23.141 (5935/25647)
HLA-DRB1*1501	35.206 (94/267)	21.836 (48671/222893)	25.891 (6584/25430)
HLA-DRB3*0101	9.158 (25/273)	8.496 (18884/222274)	6.819 (1740/25517)
HLA-DRB3*0202	18.657 (50/268)	13.832 (30687/221859)	15.843 (4059/25620)
HLA-DRB4*0101	23.529 (68/289)	12.749 (28376/222568)	16.221 (4131/25467)
HLA-DRB5*0101	23.776 (68/286)	11.235 (24993/222464)	14.648 (3732/25478)

A.5 Presentation of TMH-derived epitopes

See supplementary Table S5 for the percentage of MHC-II 14-mers overlapping with TMH.

711 **A.6 The percentage of TMH-derived epitopes from IEDB**

712 **epitopes**

713 We display the over-presentation of epitopes taken from the IEDB database, for
 714 two assays: an MHC ligand assay (Figure 2A) and a T cell assay (see figure S4),
 715 as a bar plot. Supplementary Table S6 below shows the exact numbers.

MHC class	Dataset	n
I	iedb_mhc_ligand	22.28% (1789/8030)
I	iedb_t_cell	35.91% (93/259)
II	iedb_mhc_ligand	10.46% (73/698)
II	iedb_t_cell	6.66% (42/631)

Table S6: Percentage of epitopes derived from a TMH for epitopes taken from the IEDB, for two different types of assays: an MHC ligand assay, as well as a T cell assay. The values between brackets show the the number of epitopes that were predicted to overlapping with a TMH per all epitopes that could be uniquely mapped to the representative human reference proteome.

716 A.7 Correlation of epitope presentation

717 In the main text of this research, we use two sources of epitopes to determine
 718 if TMH-derived epitopes are presented. The first source of epitopes are all the
 719 9-mers (for MHC-I) (and 14-mers for MHC-II) derived from a human reference
 720 proteome, where this over-presentation is displayed in figure 1A. The second
 721 source of epitopes are those that are present in the IEDB that are obtained
 722 from MHC ligand assays, as displayed in figure 2A.

723 Here we correlate between the over-presentation of TMH-derived epitopes
 724 between these two sources of data. Figure S3 shows per MHC allele the per-
 725 centage of TMH-derived epitopes, with a linear trendline.

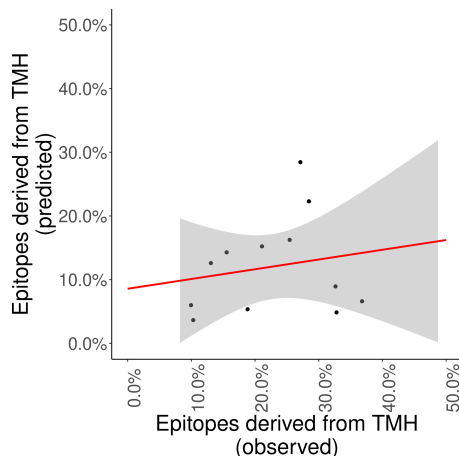


Figure S3: **TMH-derived epitopes are over-presented when using predicted as well as experimental data** For the MHC class I alleles, the over-presentation of TMH-derived epitopes is correlated between IEDB MHC ligand epitopes (horizontal axis) and the 9-mers derived from a human reference proteome (vertical axis). Alleles are listed in Table S8). The trendline shows the linear correlation between these percentages, where the gray area is the 95% confidence interval.

726 **A.8 Presentation of TMH-derived epitopes result in T cell**
727 **responses**

728 Figure S4 shows the percentage of TMH-derived epitopes of the reported epi-
729 topes from human origin for which T-cell responses were established. The data
730 was obtained from the IEDB and includes only the MHC alleles used in this
731 study. As there are many (especially class II) MHC alleles, only a small per-
732 centage of the full IEDB data could be used.

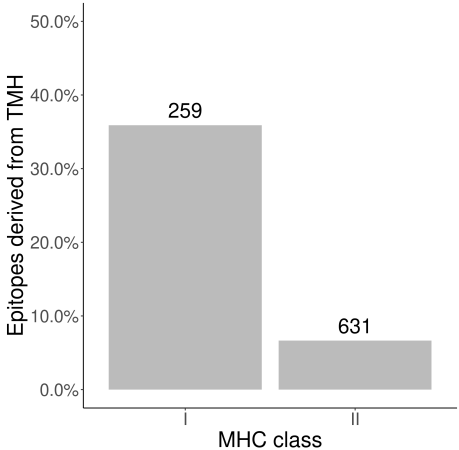


Figure S4: **TMH-derived epitopes evoke T-cell responses** The numbers above the bars denotes the number of epitopes found in the IEDB for the MHC alleles used in this study.

Table S7: Percentage of MHC-I 9-mers overlapping with TMH. Values in brackets show the number of binders that have at least one residue overlapping with a TMH (first value) as well as the number of binders (second value). percentage used: 2

haplotype	covid	human	myco
HLA-A*01:01	15.603 (44/282)	12.600 (28377/225209)	11.424 (2947/25797)
HLA-A*02:01	34.155 (97/284)	28.441 (63994/225003)	29.749 (7646/25702)
HLA-A*03:01	9.122 (27/296)	6.606 (14851/224796)	9.972 (2565/25721)
HLA-A*24:02	39.223 (111/283)	22.297 (50313/225648)	22.346 (5752/25741)
HLA-A*26:01	21.739 (65/299)	14.287 (32232/225598)	13.950 (3598/25793)
HLA-B*07:02	9.712 (27/278)	5.347 (11893/222429)	8.899 (2291/25744)
HLA-B*08:01	15.248 (43/282)	8.935 (19981/223616)	10.714 (2750/25667)
HLA-B*15:01	24.324 (72/296)	15.228 (34498/226542)	17.600 (4547/25835)
HLA-B*18:01	11.724 (34/290)	5.993 (13409/223745)	5.960 (1536/25773)
HLA-B*27:05	10.227 (27/264)	4.854 (10882/224178)	8.031 (2063/25688)
HLA-B*39:01	18.182 (50/275)	11.468 (25621/223419)	14.682 (3787/25793)
HLA-B*40:02	4.594 (13/283)	3.647 (8147/223408)	4.264 (1097/25729)
HLA-B*58:01	24.731 (69/279)	16.245 (36409/224119)	20.558 (5292/25742)

A.9 Presentation of TMH-derived epitopes

See supplementary Table S7 for the percentage of MHC-I 9-mers overlapping with TMH.

Supplementary Table S8 shows the shorthand notation for the HLA alleles.

Supplementary Tables S7 and S5 show the exact number of binders, binders that overlap with TMHs and the percentage of binders that overlap with TMHs, as visualized by figure 1A.

index	haplotype_name
1	HLA-A*01:01
2	HLA-A*02:01
3	HLA-A*03:01
4	HLA-A*24:02
5	HLA-A*26:01
6	HLA-B*07:02
7	HLA-B*08:01
8	HLA-B*18:01
9	HLA-B*27:05
10	HLA-B*39:01
11	HLA-B*40:02
12	HLA-B*58:01
13	HLA-B*15:01
1	HLA-DRB1*0101
2	HLA-DRB1*0301
3	HLA-DRB1*0401
4	HLA-DRB1*0405
5	HLA-DRB1*0701
6	HLA-DRB1*0802
7	HLA-DRB1*0901
8	HLA-DRB1*1101
9	HLA-DRB1*1201
10	HLA-DRB1*1302
11	HLA-DRB1*1501
12	HLA-DRB3*0101
13	HLA-DRB3*0202
14	HLA-DRB4*0101
15	HLA-DRB5*0101
16	HLA-DQA1*0501/DQB1*0201
17	HLA-DQA1*0501/DQB1*0301
18	HLA-DQA1*0301/DQB1*0302
19	HLA-DQA1*0401/DQB1*0402
20	HLA-DQA1*0101/DQB1*0501
21	HLA-DQA1*0102/DQB1*0602

Table S8: Abbreviations of the haplotype names

Goal	Tool	Reference
Predict topology	TMHMM	[9]
Predict topology	PureseqTM	[14]
Predict epitopes MHC-I	epitope-prediction	[7]
Predict epitopes MHC-II	NetMHCIIpan	[45, 46]
Call TMHMM from R	tmhmm	[47]
Call PureseqTM from R	pureseqtmr	[48]
Call NetMHCIIpan from R	netmhc2pan	[49]
Work with IEDB	iedbr	[50]
Work with rentrez	sprentrez	[51]
Combine all	bbbq	[52]

Table S9: Overview of all software used in this research.

740 A.10 Prediction software used

741 For this research, we needed software to predict protein topology, as well as the
742 MHC-I and MHC-II binding affinities of epitopes. We selected our software, by
743 searching the scientific literature to identify the most recent free and open source
744 (FOSS) prediction software. This was done by searching for papers that (1) cite
745 older prediction software, and (2) present a novel method to make predictions.
746 As a starting point, per type of prediction software, a review paper was used
747 ([53] for protein topology, [54] for MHC-I binding affinities and [55] for MHC-II
748 binding affinities).

749 There are multiple computational tools developed to predict which parts of
750 a protein forms a TMH. In 2001, multiple of such prediction tools have been
751 compared [53], of which TMHMM [9] turned out to be the most accurate, as
752 is used in the previous study [7]. However, TMHMM has a restrictive software
753 license and is nearly two decades old. Therefore, PureseqTM [14], was also used
754 in this study, which has been more recently developed and has a free software
755 license.

756 For MHC-I, there are multiple computational tools developed to predict epi-
757 topes. According to [54], at that time, NetMHCcons [56] gave the best predic-

758 tions. We used the same tool as used in our earlier study, **epitope-prediction**
759 [7],

760 Also for MHC-II, there are multiple computational tools developed to pre-
761 dict epitopes, such as using a trained neural network [55] or a Gibbs sam-
762 pling approach [57]. According to [54], in 2011, from a set of multiple tools,
763 NetMHCIIpan [45, 46] made the most accurate predictions. The most recent
764 FOSS tool available now appears to be MHCnuggets [20], which can do both
765 MHC-I and MHC-II predictions. As we already use **epitope-prediction** [7]
766 for MHC-I predictions, we use MHCnuggets only for MHC-II predictions.

767 To retrieve the data from the NCBI databases the **rentrez** R package [58]
768 was used that calls the NCBI database’s API. The NCBI database provides a
769 stable user experience for all users, by limiting its API to 3 calls per second
770 per user. Additionally, the API splits the result of a bigger query into multiple
771 pages, each of which needs one API call. The **sprentrez** package [51] provides
772 for bigger queries of multiple (and delayed) API calls.

773 To retrieve the data from the IEDB databases [18], the **iedbr** R package [50]
774 was written, to calls the IEDB database’s API. Similar to the NCBI database,
775 the IEDB has a limit to 1 call per second per user and allows a query results to
776 return 10k results maximally. The **iedbr** package [50] allows for bigger queries.

777 A.11 Prediction software written

778 The R programming language is used for the complete experiment, including the
779 analysis. The complete experiment is bundled in the 'bbbq' R package, which
780 is dependent on 'tmhmm', 'pureseqtmr', 'epitope-prediction' and 'mhc-nuggets-r'
781 as described below.

782 The R package 'tmhmm' was developed to do the similar topology predic-
783 tions as our earlier study (that used 'TMHMM'), yet in an automated way.
784 'TMHMM' has a restrictive software license [9] and allows a user to download a
785 pre-compiled executable after confirmation that he/she is in academia. The R
786 package respects this restriction and allows the user to install and use TMHMM
787 from within R, as done in this study. 'tmhmm' has been submitted to and is
788 accepted by the Comprehensive R Archive Network (CRAN).

789 To be able to call, from R, the TMH prediction software 'PureseqTM' [14],
790 which is written in C, the package 'pureseqtmr' has been developed. 'purese-
791 qtmr' allows to install 'PureseqTM' and use most of its features. 'pureseqtmr'
792 has been submitted to and is accepted by CRAN.

793 MHCnuggets is a free and open-source Python package to predict epitope
794 affinity for many MHC-I and MHC-II variants [20]. The R package 'mhc-
795 nuggets-r' allows one to install and use MHCnuggets from within R. Also 'mhc-
796 nuggets-r' has been submitted to and is accepted by CRAN.

797 To reproduce the full experiment presented in this paper, the functions
798 needed are bundled in the 'bbbq' R package. This package is too specific to
799 be submitted to CRAN.

Table S10: Percentage of spots and spots that overlap with a TMH

target	mhc_class	n_spots	n_spots_tmh	f_tmh
covid	1	14207	1124	7.91
covid	2	14137	1245	8.81
human	1	11220940	598391	5.33
human	2	11118448	672273	6.05
myco	1	1299707	98613	7.59
myco	2	1279742	108419	8.47

800 A.12 Prediction of percentage of epitopes overlapping with 801 a TMH

802 Supplementary Table S10 shows an overview of the findings, where a target
803 specifies the source of the proteome, where `covid` denotes SARS-CoV-2 and
804 `myco` denotes *Mycobacterium tuberculosis*. `mhc_class` denotes the MHC class,
805 `n_spots` the number of possible 9-mers (for MHC-I) or 14-mers (for MHC-II)
806 possible. `n_spots_tmh` the number of epitopes that overlapped with a TMH
807 that were binders. `f_tmh` the percentage of peptides that had at least 1 residue
808 overlapping with a TMH.

809 **A.13 Minor methods**

810 These are details that are removed from the 'Methods' section.

811 PureseqTM does not predict the topology of proteins that have less than
812 three amino acids. The TRDD1 ('T cell receptor delta diversity 1') protein,
813 however, is two amino acids long. The R package `pureseqtmr`, however, predicts
814 that mono- and di-peptides are cytosolic.

815 **A.14 Minor discussion**

816 These are details that are removed from the 'Discussion' section.

817 In this experiment we predicted epitopes that overlap with TMHs from a
818 human, bacterial and viral proteome, would these proteins be expressed in a
819 human host. Bacteria, however have different cell membranes and cell walls,
820 hence different structural requirements for a TMH. Both topology prediction
821 tools were trained to recognize human TMHs, thus we cannot be sure that
822 the transmembrane regions predicted in bacterial proteins are actually part of a
823 TMH. For the purpose of this study, we assume the error in topology predictions
824 to be unbiased way towards topology. In other words: that a bacterial TMH is
825 incorrectly predicted to be absent just as often as it is incorrectly predicted to
826 be present elsewhere.

827 Regarding the evolutionary conservation of TMHs using SNPs, again, it is
828 estimated that approximately ten percent of SNPs is a false positive that result
829 from the methods to determine a SNP. One example is that sequence variations
830 are incorrectly detected due to highly similar duplicated sequences [59]. We
831 assume that these duplications occur as often in TMHs as in regions around
832 these, hence we expect this not to affect our results.

833 In our evolutionary experiment, we removed variations that were synony-
834 mous mutations (i.e. resulted in the same amino acid, from a different genetic

code) from our analysis. There is evidence, however, that these synonymous mutations do have an effect and may even be evolutionary selected for [60]. As the possible effect of synonymous mutations is ignored by our topology prediction software, we do so as well.

839 A.15 Relative presentation of TMH-derived epitopes

840 To compare the over-presentation of TMH-derived epitopes between the differ-
 841 ent proteomes, we normalized this percentages in such a way that 1.0 is the
 842 percentage of TMH-derived epitopes that would be expected by chance. Fig-
 843 ure S5 and S6 show these normalized values for the MHC-I and MHC-II alleles
 844 respectively.

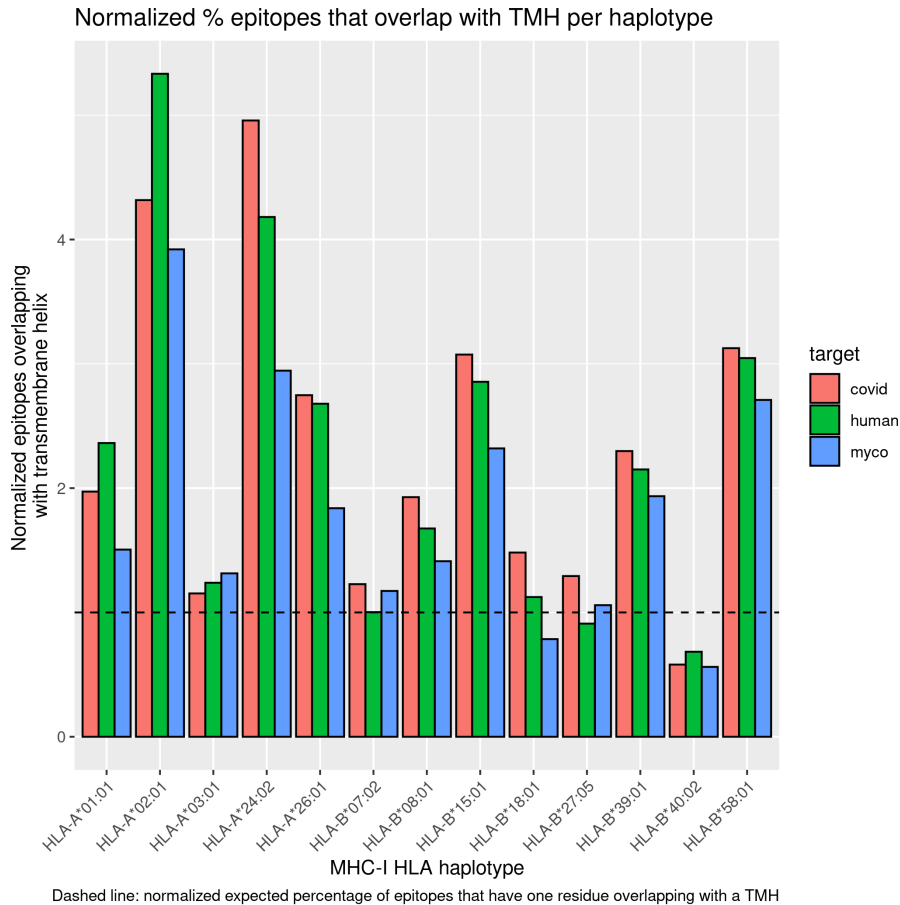


Figure S5: Normalized proportion of MHC-I epitopes overlapping with TMHs for human, viral and bacterial proteomes. Legend: covid = SARS-CoV-2, human = *Homo sapiens*, myco = *Mycobacterium tuberculosis*

845 To determine the additional over-presentation of TMH-derived epitopes in

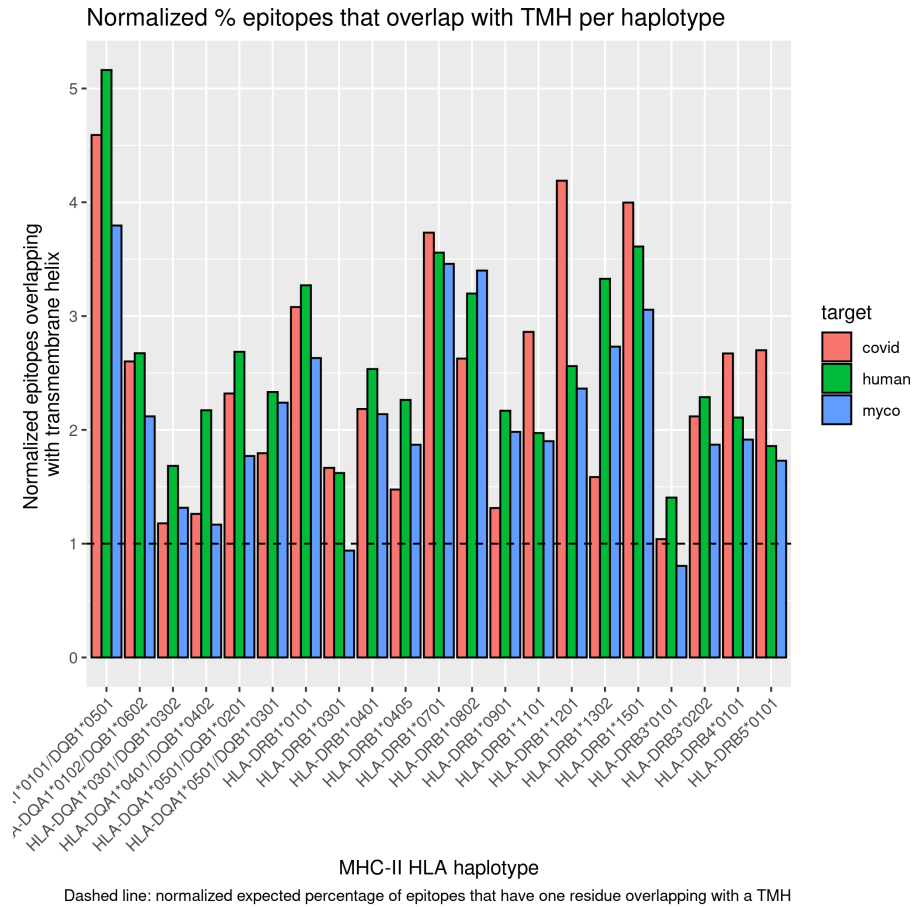


Figure S6: Normalized proportion of MHC-II epitopes overlapping with TMHs for human, viral and bacterial proteomes. Legend: covid = SARS-CoV-2, human = *Homo sapiens*, myco = *Mycobacterium tuberculosis*

846 MHC-II (as compared to MHC-I), we normalized the data to enable a side-
 847 by-side comparison. The percentage of TMH-derived epitopes presented was
 848 normalized to the expected percentage of TMH-derived epitopes, where 1.0
 849 denotes that the percentage of presented TMH-derived epitopes matches the
 850 values as expected by chance. The normalized values per MHC allele are shown
 851 in figure S7. To compare the TMH-derived over-presentation per MHC class,
 852 we grouped the normalized values per allele, and plot the mean and standard
 853 error, as shown in figure S8.

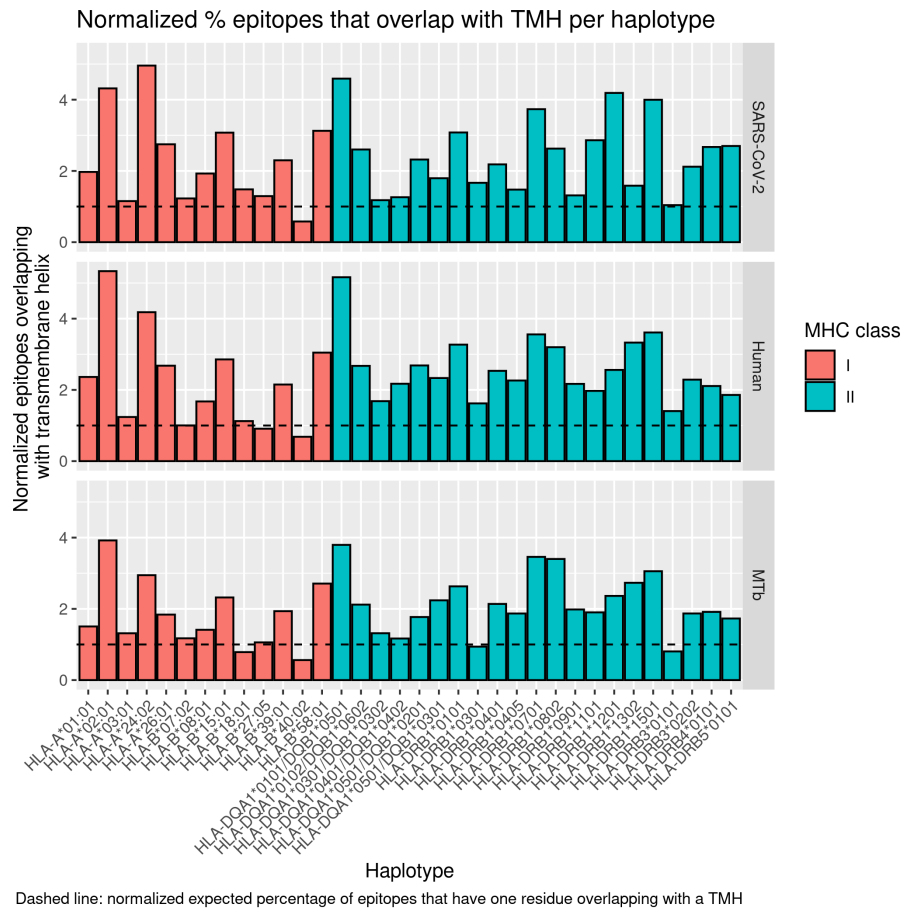


Figure S7: Normalized proportion of MHC-I and MHC-II epitopes overlapping with TMHs, for the different MHC alleles and proteomes

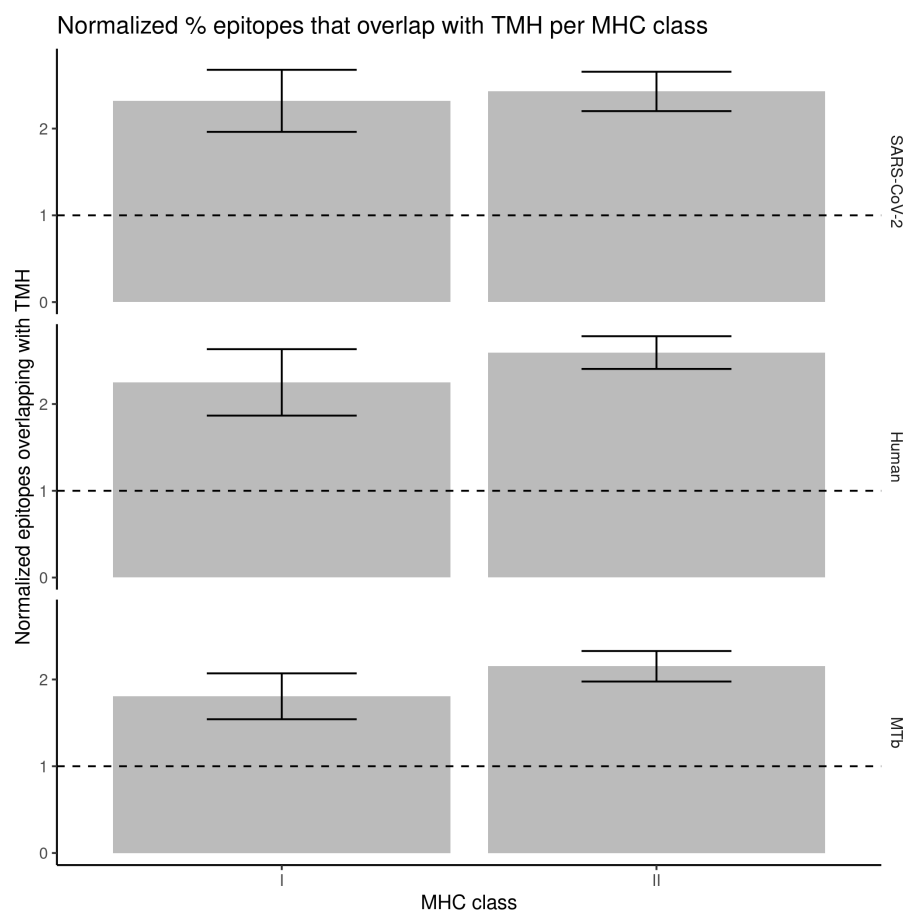


Figure S8: Normalized proportion of MHC-I and MHC-II epitopes overlapping with TMHs, for the different MHC classes and proteomes. Error bars denote the standard error.

854 **A.16 Evolutionary conservation**

855 Figure S9 shows the distribution of the number of SNPs per gene name, at the
 856 date we started the experiment, at December 14th 2020.

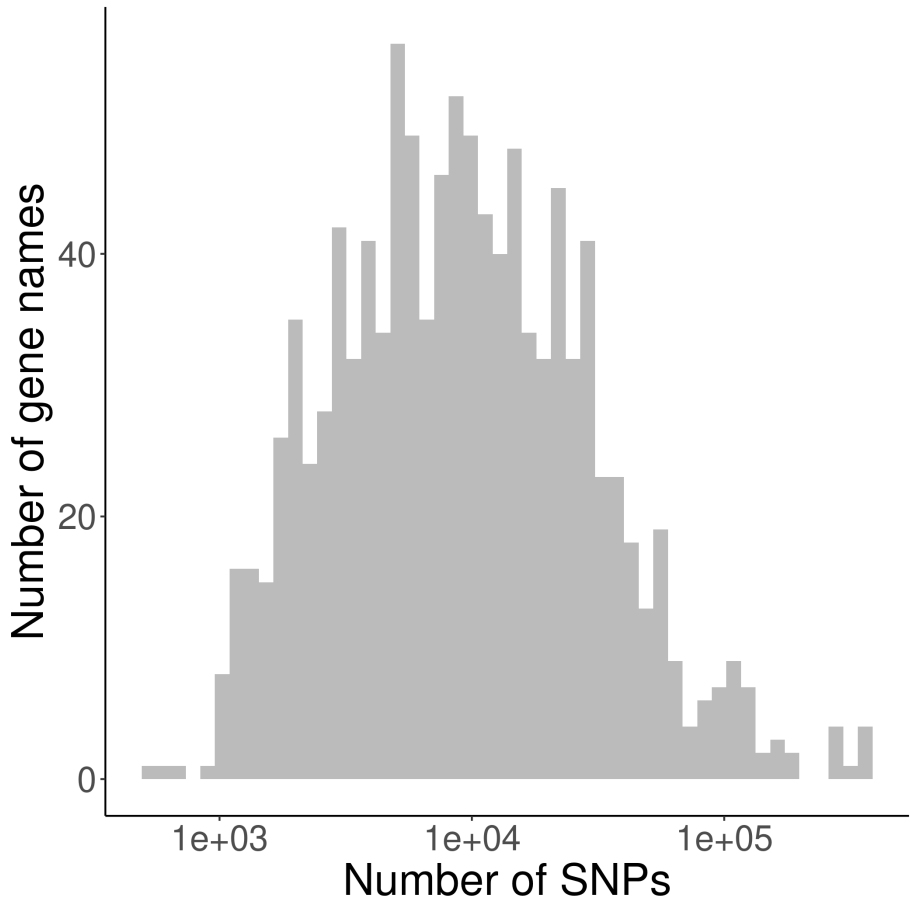


Figure S9: Distribution of the number of SNPs per gene name in the NCBI database.

857 To verify if SNPs were sampled uniformly over proteins, we show the dis-
 858 tribution of the relative position in figure S2. We find no clear evidence of a
 859 bias.

860 Supplementary Table S11 shows the statistics for all SNPs, where supple-

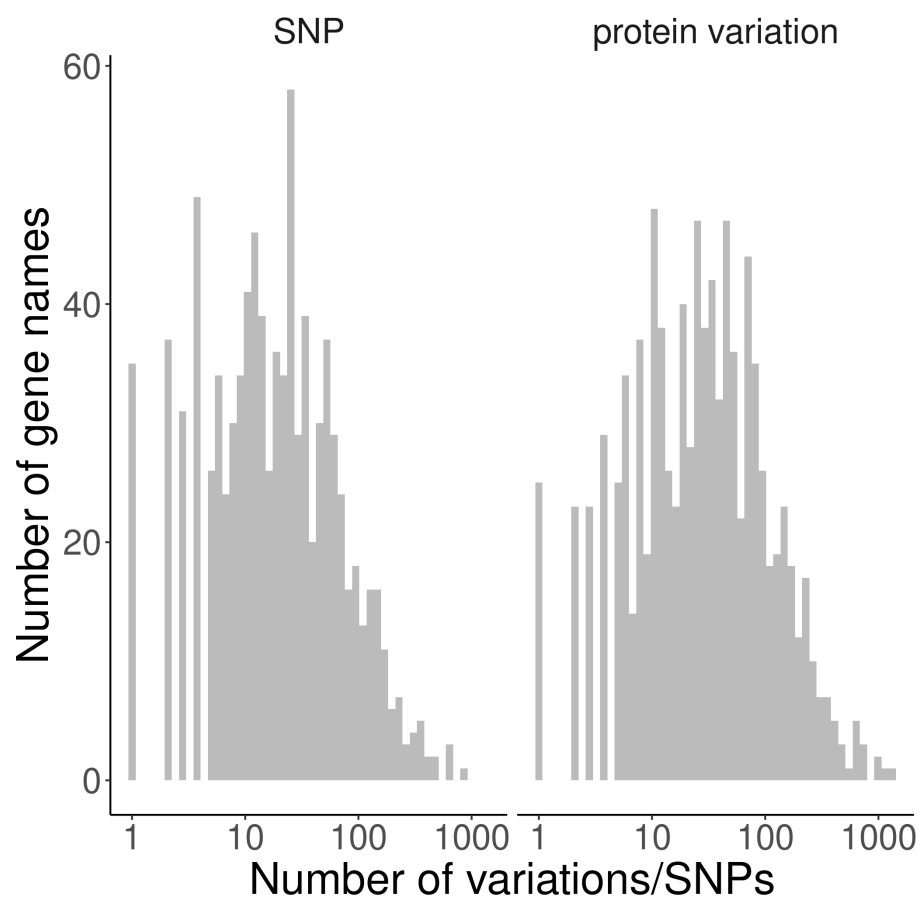


Figure S10: Distribution of the number of protein variations and SNPs per gene name processed.

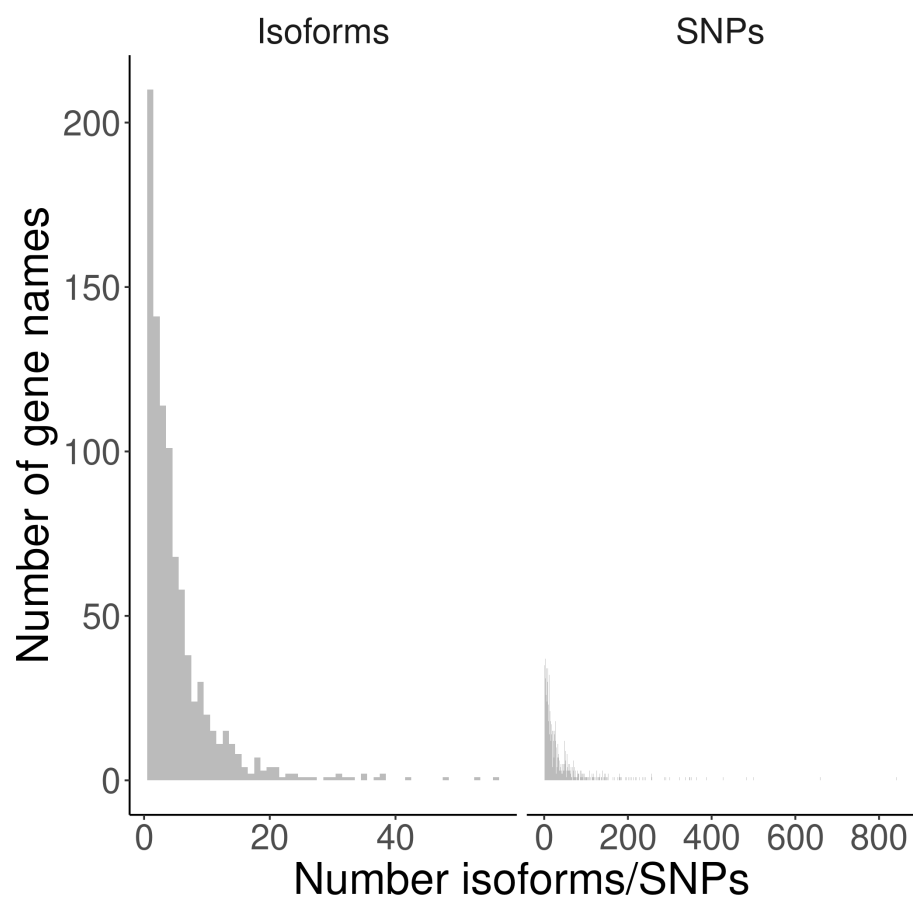


Figure S11: Histogram of the number of proteins found per gene name. Most often, a gene name is associated with one proteins.

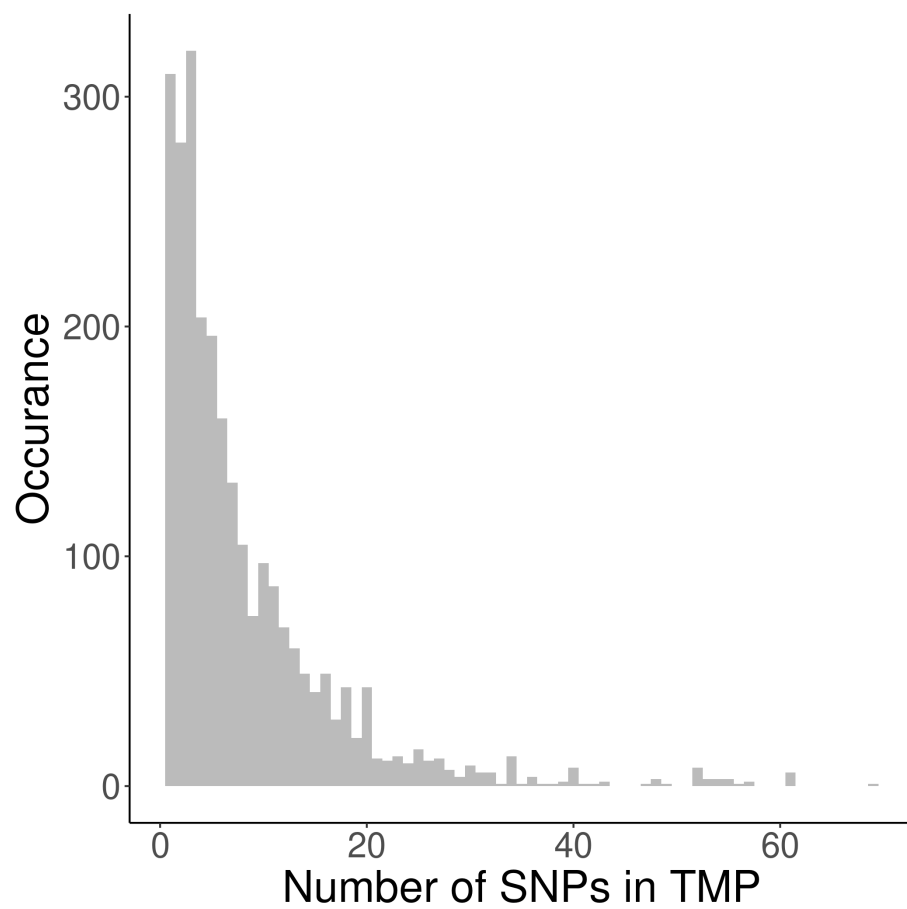


Figure S12: Histogram of the number of SNPs per trans-membrane protein.
Dashed vertical line: average number of SNPs per TMP

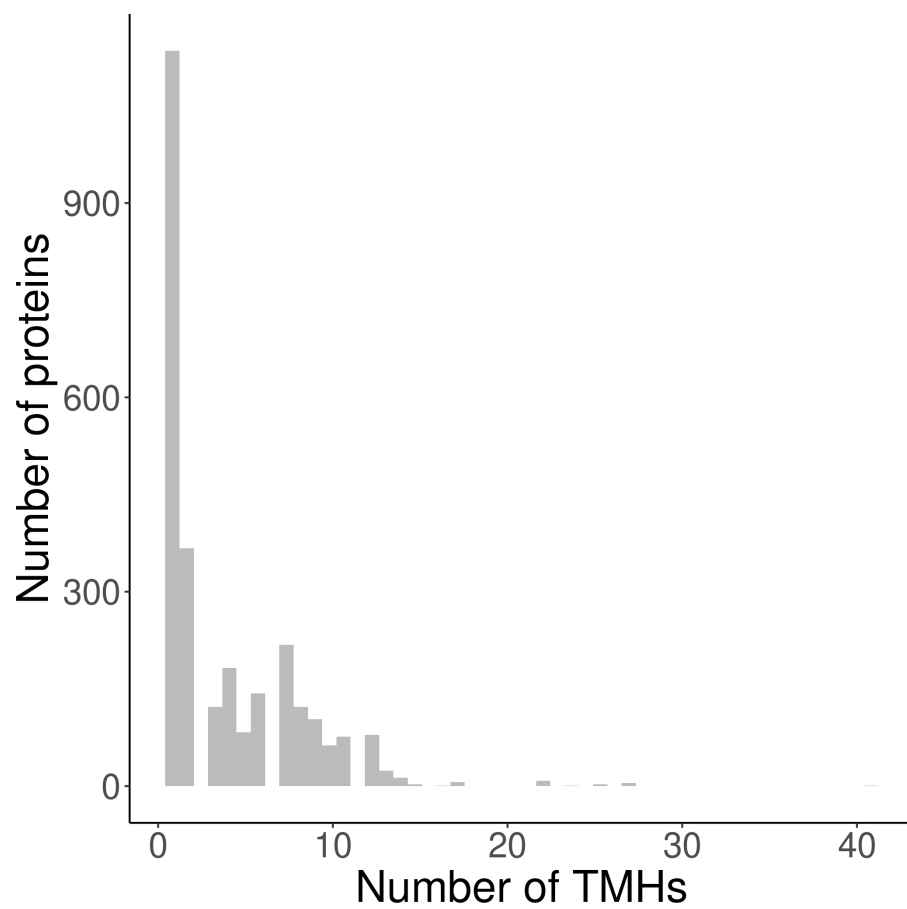


Figure S13: Histogram of the number of TMHs predicted per protein, for the trans-membrane proteins used.

Table S11: Statistics for all TMPs. p = p value. n = number of SNPs. n_{success} = number of SNPs found in TMHs (dashed blue line). $E(n_{\text{success}})$ = expected number of SNPs to be found in TMHs (dashed line).

parameter	value
p	6.820823e-11
n	21208
n_{success}	3803
$E(n_{\text{success}})$	4140.56

Table S12: Statistics for the single-spanners. p = p value. n = number of SNPs in single-spanners. n_{success} = number of SNPs found in TMHs of single-spanners (dashed blue line). $E(n_{\text{success}})$ = expected number of SNPs to be found in TMHs of single-spanners (dashed line).

parameter	value
p	0.3189532
n	8186
n_{success}	452
$E(n_{\text{success}})$	462.1535

861 mentary Tables S12 and S13 show the statistics for only single-spanners and
862 multi-spanners respectively.

Table S13: Statistics for the multi-spanners. p = p value. n = number of SNPs in multi-spanners. n_{success} = number of SNPs found in TMHs of multi-spanners (dashed blue line). $E(n_{\text{success}})$ = expected number of SNPs to be found in TMHs of multi-spanners (dashed line).

parameter	value
p	8.315841e-12
n	13022
n_{success}	3351
$E(n_{\text{success}})$	3678.406

863 **A.17 Presentation of TMH-derived epitopes when two amino** 864 **acids overlap**

865 In our experiment, we define a TMH-derived epitope as a peptide that overlaps
866 with a TMH for at least one amino acid. One could argue that we should
867 use a higher number of overlapping amino acids, so to make the epitopes more
868 'transmembrane helix-ey'. We chose not too, for two reason: (1) epitopes that
869 overlap with a TMH for 1 AA already, cannot be processed by the proteasome
870 in a known and conventional way (2) whatever number of overlapping amino
871 acids we use, we expect the pattern to be the same. However, using only 1 AA
872 gives the most TMH-derived epitopes and hence the highest statistical power.

873 To prove this point, we did exactly the same analysis as shown in Figure
874 1A, yet with defining a TMH-derived epitope as an epitope that overlaps with
875 a TMH for at least 2 AAs, as shown in Figure S14. As these two figures look
876 identical, we also added the counts as numbers, with Table S14 showing the
877 same data as S5, except the former uses 2 AAs overlap. Likewise, Table S15
878 showing the same data as S7, except the former uses 2 AAs overlap.

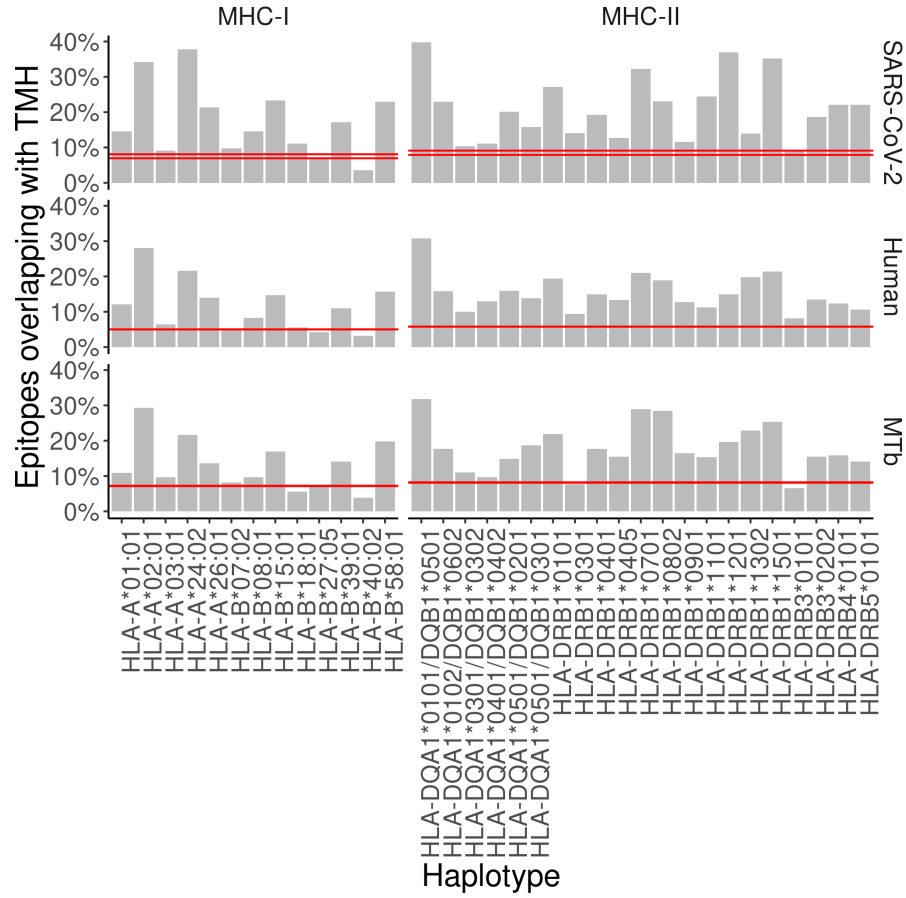


Figure S14: The percentage of epitopes for MHC-I and -II alleles that are predicted to overlap with TMHs (for at least two amino acids) for the proteomes of SARS-CoV-2 (top row), human (middle row) and *M. tuberculosis* (bottom row). The pair of dashed lines in each plot indicate the lower and upper bound of the 99% confidence interval. See supplementary Tables S14 and S15 for the exact TMH and epitope counts.

Table S14: Percentage of MHC-II 14-mers overlapping with TMH. Values in brackets show the number of binders that have at least two residues overlapping with a TMH (first value) as well as the number of binders (second value). percentage used: 2

haplotype	covid	human	myco
HLA-DQA1*0101/DQB1*0501	39.711 (110/277)	30.813 (68855/223464)	31.777 (8090/25459)
HLA-DQA1*0102/DQB1*0602	22.910 (74/323)	15.858 (35070/221147)	17.713 (4547/25671)
HLA-DQA1*0301/DQB1*0302	10.381 (30/289)	9.996 (22217/222248)	10.960 (2795/25502)
HLA-DQA1*0401/DQB1*0402	11.111 (32/288)	12.915 (28829/223219)	9.670 (2468/25522)
HLA-DQA1*0501/DQB1*0201	20.072 (56/279)	15.969 (35582/222820)	14.830 (3780/25489)
HLA-DQA1*0501/DQB1*0301	15.808 (46/291)	13.890 (30570/220089)	18.682 (4804/25715)
HLA-DRB1*0101	27.119 (80/295)	19.401 (43139/222349)	21.944 (5603/25533)
HLA-DRB1*0301	13.993 (41/293)	9.415 (20972/222752)	7.638 (1944/25451)
HLA-DRB1*0401	19.231 (55/286)	14.925 (33122/221930)	17.652 (4523/25623)
HLA-DRB1*0405	12.635 (35/277)	13.298 (29523/222012)	15.469 (3942/25484)
HLA-DRB1*0701	32.192 (94/292)	21.057 (46845/222465)	28.884 (7364/25495)
HLA-DRB1*0802	23.132 (65/281)	18.909 (41907/221623)	28.496 (7279/25544)
HLA-DRB1*0901	11.565 (34/294)	12.730 (28199/221520)	16.505 (4226/25605)
HLA-DRB1*1101	24.409 (62/254)	11.282 (25151/222928)	15.357 (3911/25467)
HLA-DRB1*1201	36.897 (107/290)	14.985 (33487/223464)	19.633 (5000/25467)
HLA-DRB1*1302	13.962 (37/265)	19.774 (44027/222646)	22.903 (5874/25647)
HLA-DRB1*1501	35.206 (94/267)	21.341 (47568/222893)	25.415 (6463/25430)
HLA-DRB3*0101	9.158 (25/273)	8.145 (18105/222274)	6.556 (1673/25517)
HLA-DRB3*0202	18.657 (50/268)	13.445 (29830/221859)	15.457 (3960/25620)
HLA-DRB4*0101	22.145 (64/289)	12.341 (27467/222568)	15.856 (4038/25467)
HLA-DRB5*0101	22.028 (63/286)	10.677 (23753/222464)	14.138 (3602/25478)

Table S15: Percentage of MHC-I 9-mers overlapping with TMH. Values in brackets show the number of binders that have at least two residues overlapping with a TMH (first value) as well as the number of binders (second value). percentage used: 2

haplotype	covid	human	myco
HLA-A*01:01	14.539 (41/282)	12.092 (27232/225209)	10.912 (2815/25797)
HLA-A*02:01	34.155 (97/284)	28.037 (63085/225003)	29.360 (7546/25702)
HLA-A*03:01	9.122 (27/296)	6.388 (14361/224796)	9.673 (2488/25721)
HLA-A*24:02	37.809 (107/283)	21.677 (48913/225648)	21.643 (5571/25741)
HLA-A*26:01	21.405 (64/299)	13.905 (31370/225598)	13.632 (3516/25793)
HLA-B*07:02	9.712 (27/278)	4.880 (10854/222429)	8.184 (2107/25744)
HLA-B*08:01	14.539 (41/282)	8.218 (18376/223616)	9.662 (2480/25667)
HLA-B*15:01	23.311 (69/296)	14.686 (33269/226542)	16.961 (4382/25835)
HLA-B*18:01	11.034 (32/290)	5.603 (12537/223745)	5.560 (1433/25773)
HLA-B*27:05	6.818 (18/264)	4.171 (9350/224178)	7.054 (1812/25688)
HLA-B*39:01	17.091 (47/275)	10.983 (24538/223419)	14.159 (3652/25793)
HLA-B*40:02	3.534 (10/283)	3.251 (7264/223408)	3.852 (991/25729)
HLA-B*58:01	22.939 (64/279)	15.627 (35022/224119)	19.793 (5095/25742)

879 **B** Figures

880 **Figure 1: Over-presentation of TMH-derived epitopes on most**
 881 **MHC-I and -II alleles (A)** The percentage of epitopes for MHC-I and -II
 882 alleles that are predicted to overlap with TMHs for the proteomes of SARS-
 883 CoV-2 (top row), human (middle row) and *M. tuberculosis* (MtB; bottom row).
 884 The pair of horizontal red lines in each plot indicate the lower and upper bound
 885 of the 99% confidence interval. See supplementary Tables S5 and S7 for the
 886 exact TMH and epitope counts. **(B-C)** Correlation between the percentages of
 887 predicted TMH-derived epitopes and the hydrophobicity score of all predicted
 888 epitopes for human MHC-I **(B)** and MHC-II alleles **(C)**. Diagonal red line:
 889 linear regression analysis. Labels are shorthand for the HLA alleles, see the
 890 supplementary Table S8 for the names.

891 **Figure 2: Analysis of epitope database shows that TMH derived**
892 **epitopes are over presented.** The percentage of epitopes for MHC-I and -II
893 alleles that overlap with TMHs that are presented. The pair of horizontal red
894 lines in each plot indicate the lower and upper bound of the 99% confidence
895 interval. Note that only one line is visible as this interval is relatively narrow.
896 Alleles are listed in Table S8). **(A)** Observed and predicted percentage of TMH-
897 derived epitopes for MHC-I alleles. **(B)** MHC ligands from IEDB corresponding
898 to TMH-derived epitopes. The numbers above the bars denotes the number of
899 TMH derived epitopes obtained.

900 **Figure 3: Evolutionary conservation of human TMHs.** (A) Percent-
 901 age of SNPs found in TMHs. Each point shows for one protein the predicted
 902 percentage of amino acids that are part of a TMH (x -axis) and the observed
 903 occurrence of SNPs being located within a TMH (y -axis). The dashed diagonal
 904 line shows the line of equality (i.e., equal conservation of TMHs and soluble
 905 protein regions). The diagonal red line indicates a linear fit, the gray area its
 906 95% confidence interval. (B) Distribution of the percentages of TMH in the
 907 TMPs used in this study. (C) The number of SNPs in TMHs as expected by
 908 chance (left bar) and found in the dbSNP database (right bar). Percentages
 909 show the relative conservation of SNPs in TMHs found relative to stochastic
 910 chance.

911 **Figure 4: Membrane proteins with multiple TMHs are evolution-**
 912 **ary more conserved than proteins with only a single TMH. (A)** Percent-
 913 age of SNPs found in TMPs predicted to have only a single (left) or multiple
 914 (right) TMHs. Each point shows for one protein the predicted percentage of
 915 amino acids that are part of a TMH (x -axis) and the observed occurrence of
 916 SNPs being located within a TMH (y -axis). The dashed diagonal lines show the
 917 line of equality (i.e., equal conservation of TMHs and soluble protein regions).
 918 The diagonal red lines indicate a linear fit, the gray areas their 95% confidence
 919 intervals. **(B)** The number of SNPs in TMHs as expected by chance and ob-
 920 served in the dbSNP database, for TMPs with one TMH (single-spanners) and
 921 multiple TMHs (multi-spanners). Percentages show the relative conservation of
 922 SNPs in TMHs found relative to the stochastic chances. **(C)** Distribution of
 923 the proportion of amino acids residing in the plasma membrane.